



Norwegian University of
Science and Technology

Model Testing and Rheology of a Fine Grain Rich Debris Flow

Åmund Hognestad

Civil and Environmental Engineering

Submission date: June 2018

Supervisor: Vikas Kumar Singh Thakur, IBM

Co-supervisor: Steinar Nordal, IBM

Norwegian University of Science and Technology
Department of Civil and Environmental Engineering



Report Title: Model Testing and Rheology of a Fine Grain Rich Debris Flow	Dato: 11.06.2018	
	Number of pages: 97	
	Master Thesis	<input checked="" type="checkbox"/>
Name: Åmund Skjørshammer Hognestad		
Professor in charge/supervisor: Vikas Thakur		
Other external professional contacts/supervisors:		

Abstract:

Debris flows are a hazardous type of landslide, primarily caused by intense precipitation in steep mountainous terrain. Water, soil and debris mix to form a slurry that advances rapidly downslope, growing in size as it entrains more and more mass. They occur all over the world and are prevalent in canyons and steep gullies. They are considered to be one of the most dangerous landslide types, due poor predictability, a rapid onset, high mobility and high destructive powers.

To investigate the flow behaviour of fine grain rich debris flow, rheological experiments and physical modeling has been conducted. The rheology has primarily been investigated using viscometer testing. Six viscometer tests were conducted. It was shown that fine grain rich soil material behaved as a shear thinning material exhibiting a yield strength and could be modeled using Herschel-Bulkley rheology.

22 flume model tests were conducted using the same, fine grain rich material as for the viscometer tests. Velocities, flow heights and impact forces were measured and analysed. Two different soils were used, where the primary difference was the size of the clay fraction. Tests were conducted using different solid concentrations and quickness values. Coefficients for two simple hydraulic models (static and dynamic) were calculated from the results. The results indicate that the effect of variations in quickness value or solid concentration decreases as the flow volume is increased. The effect variations in quickness value appears to be complex. An extremum for the middle quickness value was observed in the velocity, flow height and impact force results. This implies that at least two effects are acting against each other when the quickness value is increased.

Keywords:

1. Debris Flow
2. Viscometer testing
3. Physical modeling
4. Rheology

(sign.)

**MASTER DEGREE THESIS**

Spring 2018

for

Student: Åmund Skjørshammer Hognestad

Model Testing and Rheology of Fine Grain Rich Debris Flow**BACKGROUND**

Debris flows are a hazardous type of landslide, primarily caused by intense precipitation in steep mountainous terrain. Water, soil and debris mix to form a slurry that advances rapidly downslope, growing as it entrains more and more mass. They occur all over the world and are prevalent in canyons and steep gullies. They are considered to be one of the most dangerous landslide types, due poor predictability, a rapid onset, high mobility and high destructive powers. An example of recent disasters is the 2018 Southern California debris flows, which caused at least 21 fatalities \citep{dolan_2018} and 177 million USD in property damages. To understand the mechanisms and magnitudes of debris flows, systematic research is needed. Due to the unpredictable nature of debris flows it is difficult to obtain good quality data from natural events. To control a debris flow event from the initiation to when it comes to rest, physical models can be used. However, full-scale models are costly and time-consuming to operate, necessitating the use of small-scale models. In order to use miniaturised models, the effects of scaling must be accounted for. Numerical modeling can also be used to compute and simulate debris flow events. As a debris flow behaves as a continuous fluid, numerical models based on fluid dynamics can be used. This requires a description of the rheological behaviour of the debris flow material, which can be obtained through viscometric testing.

TASK

The aims of this master thesis are to investigate the rheological behavior of fine grain rich debris flow, and to conduct experiments in a physical flume model.

Task description

- Literature review on debris flow, flume modeling and rheological behavior of debris flow.
- Flow behavior testing, including quickness and viscometer testing.
- Conduct flume model experiments.
- Analyse the results and compare them to previous findings in literature.

Professor in charge:

Prof. Vikas Thakur

Department of Civil and Transport Engineering, NTNU

Date: 11.06.2018

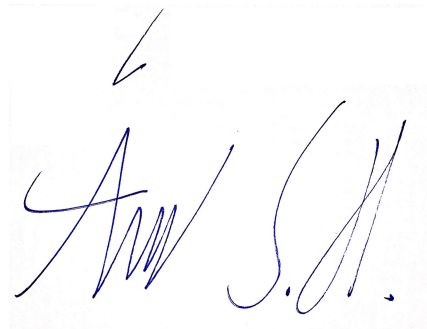
Preface

This master thesis is written as part of the Master of Science degree in Civil and Environmental Engineering at the Norwegian University of Science and Technology (NTNU) in Trondheim. The thesis has been written during the spring semester of 2018, between January and June.

The thesis contains a literary review of current and historical research into debris flows. The test program and experimental procedures are described, along with the results and critical discussion. The report is intended for readers with a basic knowledge in geotechnics.

The concept for this thesis was developed by my supervisor, Professor Vikas Thakur, as a study into the behaviour of fine grain rich debris flows.

Trondheim, 2018-06-11

A handwritten signature in blue ink, consisting of the initials 'ÅS' followed by a full name, written in a cursive style. The signature is placed on a light-colored rectangular background.

Åmund Skjørshammer Hognestad

Acknowledgment

I am very thankful to my supervisor Vikas Thakur for his encouragement and guidance, as well as for connecting me with the right people necessary to fulfill the work done in this thesis. I am grateful to Einar Husby, Karl-Ivar Volden Kvisvik and Espen Andersen for helping with acquiring the soil material needed, as well as for fixing anything that went wrong with the model. I would like to thank Per Østbye for help with the computer logger. I would also like to thank Erik Larsen for providing the viscometer. I am grateful to Alex Klein-Paste for letting me borrow the Phantom high-speed camera, and to Henri Giudici for teaching me how to operate it. I am also grateful for the discussion with Petter Fornes about viscometer results. I am especially grateful to PhD Candidate Ashenafi Lulseged Yifru for help with the planning and execution of the experiments, as well as being available in discussion of a great number of things. I would also like to give a special thanks to fellow Master's student Hervé Vicari for spending time helping me conduct the experiments, and being available for discussion of the results afterwards.

Å.S.H.

Abstract

Debris flows are a hazardous type of landslide, primarily caused by intense precipitation in steep mountainous terrain. Water, soil and debris mix to form a slurry that advances rapidly downslope, growing in size as it entrains more and more mass. They occur all over the world and are prevalent in canyons and steep gullies. They are considered to be one of the most dangerous landslide types, due poor predictability, a rapid onset, high mobility and high destructive powers.

To investigate the flow behaviour of fine grain rich debris flow, rheological experiments and physical modeling has been conducted. The rheology has primarily been investigated using viscometer testing. Six viscometer tests were conducted. It was shown that fine grain rich soil material behaved as a shear thinning material exhibiting a yield strength, and could be modeled using Herschel-Bulkley rheology.

22 flume model tests were conducted using the same, fine grain rich material as for the viscometer tests. Velocities, flow heights and impact forces were measured and analysed. Two different soils were used, where the primary difference was the size of the clay fraction. Tests were conducted using different solid concentrations and quickness values. Coefficients for two simple hydraulic models (static and dynamic) were calculated from the results. The results indicate that the effect of variations in quickness value or solid concentration decreases as the flow volume is increased. The effect variations in quickness value appears to be complex. An extremum for the middle quickness value was observed in the velocity, flow height and impact force results. This implies that at least two effects are acting against each other when the quickness value is increased.

Sammendrag

Flomskred er svært farlig form for skred, og er hovedsakelig forårsaket av perioder med kraftig nedbør i bratt terreng. Vann, jord og avfall danner en blanding som sklir meget raskt nedover terrenget, samtidig som det tar opp mer masse underveis. Flomskred opptrer over hele verden, særlig i steile daler og bratte fjellsider. Det blir sett på som en av de farligste skredtypene, og er preget av lite forutsigbarhet, plutselige oppstandelse, høye hastigheter og en enormt destruktiv kraft.

Reologiske eksperimenter og fysisk modellering ble gjennomført for å undersøke egenskapene til et flomskred bestående av en høy andel finkorn. Reologien har primært blitt undersøkt ved hjelp av viskometerforsøk. Seks viskometerforsøk har blitt utført. Det ble vist at flomskred med en høy andel av finkorn oppfører seg som et skjærtynnende materiale med en flytespenning, og kunne modelleres ved hjelp av Herschel-Bulkley-reologi.

22 modellforsøk i en ble utført i en skredmodell. Det samme finkornige materialet ble brukt her som i viskometerforsøkene. Hastigheter, flyte høyder og krefter ble målt og analysert. To ulike jordtyper ble brukt, hvor den største forskjellen var størrelsen på leirfraksjonen. Forsøkene ble utført med ulike konsentrasjoner av faststoff og kvikkhetsverdier. Koeffisienter til to enkle, hydrauliske modeller (statisk og dynamisk) ble regnet ut. Resultatene indikerer at effekten av variasjon i kvikkhetsverdi eller konsentrasjon minker dersom volumet øker. Effekten av en variasjon i kvikkhetsverdi er tilsynelatende kompleks. Et ekstremalpunkt i resultatene for den midterste kvikkhetsverdien ble observert i resultatene. Dette impliserer at minst to ulike effekter jobber mot hverandre når kvikkhetsverdien økes.

Contents

Preface	i
Acknowledgment	ii
Abstract	iv
1 Introduction	3
1.1 Background	3
1.2 Objectives	4
1.3 Structure of the Report	4
2 Literature Review	7
2.1 Debris Flow	7
2.1.1 Classification of Debris Flow	9
2.1.2 Triggering Factors and Mechanisms	10
2.1.3 Physics of Debris Flow	11
2.2 Flow Behaviour of Fine-grained Debris Flows	12
2.2.1 Remoulded Shear Strength	12
2.2.2 Quickness	12
2.2.3 Rheology	14
2.2.4 Rheological Models for Fine Grain Rich Debris Flows	16
2.2.5 Herschel-Bulkley Model	16
2.2.6 Viscometry in Debris Flow Research	18
2.2.7 Previous Studies On Herschel-Bulkley Parameters for Fine-Grained Debris Flows	21

2.3	Physical Modeling of Debris Flow	23
2.3.1	Small-scale Theory	23
2.4	Analytical Models for estimating Debris Flow Impact Forces	24
3	Laboratory Experiments	27
3.1	Test Material	27
3.1.1	Grain Size Distribution	28
3.1.2	Dry Density	28
3.2	Flow Behaviour Testing	29
3.2.1	Sample Preparation	30
3.2.2	Remoulded Shear Strength	30
3.2.3	Quickness Test	30
3.2.4	Viscometer Test	32
3.3	Flume model testing	36
3.3.1	Flume Model at NTNU	36
3.3.2	Instrumentation	39
3.3.3	Expected Range of Results	42
3.3.4	Test plan	43
3.3.5	Test procedure	45
4	Processing of Test Data	47
4.1	Viscometer data processing	47
4.2	Flume Model Test Data	49
4.2.1	Video Analysis	49
4.2.2	Flow Height Data Analysis	51
4.2.3	Force Sensor Data Analysis	53
4.3	Coefficients for Debris Flow Impact Formulas	54
5	Results	55
5.1	Flow Behaviour Tests	55
5.1.1	Fall Cone Test Results	55
5.1.2	Quickness Test Results	56

5.1.3	Viscometer Test Results	56
5.2	Flume model test results	59
5.2.1	Velocity and Flow Height	60
5.2.2	Impact Force	63
5.2.3	Coefficients for use in Analytical Solutions	64
5.2.4	Impact Force of a Solid Clump of Soil	65
6	Discussion	69
6.1	Quickness and Remoulded Shear Strength	69
6.2	Viscometer test	69
6.3	Physical Modeling of Debris Flow	73
6.3.1	Velocity	74
6.3.2	Flow Height	74
6.3.3	Froude Number	75
6.3.4	Impact Forces	75
6.4	Analytical models for estimating impact forces	76
6.5	Effect of Flow Volume in the Flume Model	77
6.6	Effect of Quickness	80
6.7	Effect of an increased Clay Fraction	83
7	Conclusion and Further Work	85
7.1	Conclusions	85
7.2	Recommendations for Further Work	86
	Bibliography	88
A	Additional Results from Viscometer Testing	95
B	Additional Results from Flume Modeling	97

List of Figures

2.1	Classification of landslides. Facsimile from Hungr et al. (2001). Debris flow highlighted in yellow.	8
2.2	Examples on quickness test results on remoulded sensitive clays. Corresponding remoulded shear strength and quickness values (Q) are shown below each test. Figure is taken from Thakur and Degago (2012).	13
2.3	Example of flow curves for a Newtonian fluid, and non-Newtonian fluids with shear thinning and shear thickening behaviour.	15
2.4	Example of how the Bingham model is fitted to experimental data.	17
2.5	Schematic of a coaxial rotational viscometer. The spindle rotates at a certain rotational velocity and measures the torque acting on the spindle.	19
3.1	Grain size distribution curves for soil 1 and soil 2.	28
3.2	Quickness test procedure, taken from Thakur and Degago (2012)	31
3.3	Picture of the before and after a quickness test. The test in the photograph is an example test and not part of the test program.	31
3.4	Bohlin Visco 88 BV Viscometer	33
3.5	Picture of the flume model at NTNU.	37
3.6	The runout channel. Flow height sensors are circled.)	38
3.7	The mixer used to mix and release the debris flow material.)	39
3.8	Sketch of the flume model with instrumentation (all linear dimensions are in meters)	40
3.10	A) Flow height sensor. B) Phantom VEO 410L High-speed camera. C) Impact area of force sensor. D) Pore pressure sensor.	42

4.1	Two different rotational viscometer design principles. Left: Inner spindle rotates with angular velocity ω . Right: Outer cylinder rotates with angular velocity ω . The drawn velocity profile is only an illustration of non-linear velocity profile.	48
4.2	Effect of barrel distortion illustrated. The red arrows are equal in length, in reality the distance between each of the white stripes is 10 cm.	50
4.3	Still images from videos recorded at different frame rates.	51
4.4	Example of flow height sensor data, showing how peak flow height is selected. . . .	52
4.5	A typical force sensor signal. In general, the peak impact is taken as the max impact force. The opening of the mixer and release of the material is visible due to the vibrations it causes in the model.	53
5.1	Results from the dynamic response test. Torque readings for different rotational speeds.	57
5.2	Screenshots from high-speed recording of test set 6 (Q77S1V20), illustrating that the composition of the flow remains the same in the front and the middle of the flow, and that no noticeable segregation occurs during the test.	59
5.3	Screenshots from high-speed recording of test set 6 (Q77S2V40), showing the interaction with the force sensor. The flow becomes highly turbulent and is spraying upwards as it hits the sensor.	61
5.4	Typical flow height results, from test Q85S1V20-1.	63
5.5	66
5.6	The signal from the force sensor for test Q77S2V40-2. Notice the impact force being significantly larger than the max impact force of the fluid	67
6.1	Flow curves plot of the results from this thesis with select flow curves from Major and Pierson (1992) and Adamson (2017).	70
6.2	Herschel-Bulkley flow curves for all tests. The equation for the Herschel-Bulkley model is $\tau = \tau_y + K\dot{\gamma}^n$	71
6.3	Picture of inside the bowl with leftover material from a viscometer test. Notice the water visible in the shaded region.	72
6.4	Curve fit of test C40S1. The curve fitted to all points was considered the best fit . . .	73

6.5 77

6.6 Release volume plotted against max impact force. Average for test set 1–6. 78

6.7 80

6.8 81

6.9 C_s vs impact force for all test sets, including the additional test sets. Average values. 82

6.10 Test using soil 2 with a C_s of 35%. 83

List of Tables

2.1	Selected Herschel-Bulkley parameters from Major and Pierson (1992). Clay and silt mixed with sand.	22
2.2	Herschel-Bulkley parameters for different soils. Testing done at ca 7°C. From Adamson (2017). *The silt material had problems with segregation during testing.	22
3.1	Table of solid concentrations used for flow behaviour tests (remoulded shear strength, quickness and viscosity	29
3.2	Speed settings on the Bohlin Visco 88 BV	34
3.3	Dimensions of the viscometer spindle and cylinder pair used in the experiments. .	34
3.4	Test plan for the flume model testing. Test set 7 and 8 consists of only one repetition each.	44
5.1	Results from the fall cone tests. "-" indicates the material was too liquid for an indentation.	56
5.2	Results from the quickness test	56
5.3	Best-fit curve parameters and the corresponding Herschel-Bulkley parameters. . .	58
5.4	Velocities, flow heights, calculated flow discharges and Froude numbers. Discharge and Froude number is calculated using the maximum flow height recorded 1 m before the end of the runout channel.	62
5.5	Corrected impact force values, as well as calculated impact pressure for all successful tests.	64
5.6	Calculated analytical hydrostatic and hydrodynamic coefficients for all successful test repetitions.	65

6.1 Results for the 40 L tests, average of test repetitions. 79

6.2 Quickness values and their associated solid concentrations for soil 1 and soil 2.
Quickness values of 93% and 95% were practically the same. 83

A.1 Curve fit parameters for all tests. Curves are fitted to the equation $T = H_{HB}N^J + G_{HB}$ 95

B.1 Velocities as calculated from videos. Position is given relative to the force sensor
at 0 m. 97

Chapter 1

Introduction

1.1 Background

Debris flows are a hazardous type of landslide, primarily caused by intense precipitation in steep mountainous terrain. Water, soil and debris mix to form a slurry that advances rapidly downslope, growing in size as it entrains more and more mass. They occur all over the world, and are prevalent in canyons and steep gullies. They are considered to be one of the most dangerous landslide types, due poor predictability, a rapid onset, high mobility and high destructive powers. An example of recent disasters is the 2018 Southern California debris flows, which caused at least 21 fatalities (Dolan, 2018) and 177 million USD in property damages.

In order to understand the mechanisms and magnitudes of debris flows, systematic research is needed. Due to the unpredictable nature of debris flows it is difficult to obtain good quality data from natural events. In order to control a debris flow event from the initiation to when it comes to rest, physical models can be used. However, full-scale models are costly and time-consuming to operate, necessitating the use of small-scale models. In order to use miniaturised models, the effects of scaling must be accounted for.

Numerical modeling can also be used to compute and simulate debris flow events. As a debris flow behaves as a continuous fluid, numerical models based on fluid dynamics can be used. This requires a description of the rheological behaviour of the debris flow material, which can

be obtained through viscometric testing.

1.2 Objectives

The main objectives of this thesis are

1. Understand the physics of debris flows using a flume model available at NTNU.
2. Investigate the flow properties of fine-grained debris flow material using viscometer testing.
3. Study the impact of flow volume, quickness and concentration on the velocity, flow height and impact forces of a fine-grained debris flow using the flume model.
4. Critically assess the test results the conducted experiments in comparison with reported findings in the literature.

1.3 Structure of the Report

The rest of the report is structured as follows:

Chapter 2 is a literature review consisting of four parts. The first part gives a brief introduction to debris flows in general. The second part contains theory and experimental methods for describing flow properties of fine-grained soil. The third and fourth part gives an introduction to small-scale theory used in physical modeling of debris flow, as well as an overview of selected analytical models for estimating impact forces. Findings from previous experiments on physical modeling of debris flows are also given.

Chapter 3 gives a description of all laboratory experiments conducted in this thesis, including principles, test program and methods.

Chapter 4 details methods used to process the test data from viscometer tests and the flume model tests.

Chapter 5 presents the results from the conducted experiments.

Chapter 6 discusses the results from the experiments. Results are compared to previous studies and expected findings. The ability of the flume model experiments to represent a real debris flow is evaluated. Relationships between volume, quickness and concentration, as well as the effect of the clay content is investigated.

Chapter 7 is a conclusion to the study, and also contains suggestions for further work.

Chapter 2

Literature Review

The first two sections of this chapter is based on Hognestad (2017).

2.1 Debris Flow

Various definitions of a debris flow exists in the literature, but generally, it can be said that it is a mixture of water and sediment that flows as if it was a continuous fluid driven by gravity (Takahashi, 2014). An important aspect is that a debris flow resembles a viscous liquid in its behaviour, as opposed to other types of landslides. A key component in a debris flow is water, and often a slide can transform into a flow, depending on the water content and evolution of the movement.

The immense destructive capabilities of debris flows comes from the fact that they have a rapid onset, with a very fast movement speed and can contain large boulders and other large, destructive pieces of debris. Typical velocities range up to 5-15 m/s, with a magnitudes of 10^3 - 10^6 m³ and an arrival distance of up to 10 km (Hung et al., 2001)(Highland and Bobrowsky, 2008)(Laache, 2016).

The classification of debris flows and other landslides of the flow type varies, and there are many variations, especially when language differences are taken into account. The different definitions focuses on the involved material, on the water saturation and on the velocity of the flow.

Hungr et al. (2001) proposes a definition of "debris" as loose *unsorted* material of low plasticity, such as weathering, glacier transport, explosive volcanism or unsorted anthropogenic waste. It can also contain organic material, such as logs or tree stumps. This distinguishes it from e.g. *mud*, which is soft, remoulded clayey soils that are significantly plastic (Plasticity Index > 5%). Figure 2.1 shows a classification of different landslide types from Hungr et al. (2001).

Classification of Landslides

Table 4. Classification of landslides of the flow type.

Material	Water Content ¹	Special Condition	Velocity	Name
Silt, Sand, Gravel, Debris (talus)	dry, moist or saturated	- no excess pore-pressure, - limited volume	various	Non-liquefied sand (silt, gravel, debris) flow
Silt, Sand, Debris, Weak rock ²	saturated at rupture surface content	- liquefiable material ³ , - constant water	Ex. Rapid	Sand (silt, debris, rock) flow slide
Sensitive clay	at or above liquid limit	- liquefaction <i>in situ</i> , ³ - constant water content ⁴	Ex. Rapid	Clay flow slide
Peat	saturated	- excess pore-pressure	Slow to very rapid	Peat flow
Clay or Earth	near plastic limit	- slow movements, - plug flow (sliding)	< Rapid	Earth flow
Debris	saturated	- established channel ⁵ , - increased water content ⁴	Ex. Rapid	Debris flow
Mud	at or above liquid limit	-fine-grained debris flow	> Very rapid	Mud flow
Debris	free water present	- flood ⁶	Ex. Rapid	Debris flood
Debris	partly or fully saturated	- no established channel ⁵ , - relatively shallow, steep source	Ex. Rapid	Debris avalanche
Fragmented Rock	various, mainly dry	- intact rock at source, - large volume ⁷	Ex. Rapid	Rock avalanche

¹ Water content of material in the vicinity of the rupture surface at the time of failure.

² Highly porous, weak rock (examples: weak chalk, weathered tuff, pumice).

³ The presence of full or partial *in situ* liquefaction of the source material of the flow slide may be observed or implied.

⁴ Relative to *in situ* source material.

⁵ Presence or absence of a defined channel over a large part of the path, and an established deposition landform (fan). Debris flow is a recurrent phenomenon within its path, while debris avalanche is not.

⁶ Peak discharge of the same order as that of a major flood or an accidental flood. Significant tractive forces of free flowing water. Presence of floating debris.

⁷ Volume greater than 10,000 m³ approximately. Mass flow, contrasting with fragmental rock fall.

Figure 2.1: Classification of landslides. Facsimile from Hungr et al. (2001). Debris flow highlighted in yellow.

Other definitions of debris flow are more general, Highland and Bobrowsky (2008) defines it as a rapid mass movement of a slurry containing loose soil, organic matter and rocks, including

large boulders.

2.1.1 Classification of Debris Flow

Debris flows can be divided into different types. The Norwegian Public Road Administration (NPRA) distinguishes between two different types, the turbulent debris flow and the fully developed debris flow (Vegdirektoratet, 2014):

A **turbulent debris flow** is characterized by a high velocity and high amount of water, where the turbulence is lifting up the particles. The transport capacity increases with the turbidity. This type of debris flow mostly occurs in areas where there is a lot of fine material, such as close to glaciers and in volcanic regions.

A prerequisite for a high turbidity is a low volumetric concentration of solids. Thus, turbulent debris flows will usually have a volumetric concentration of solids (C_s) lower than 30%, and 75% of the particles will be smaller than 1 mm in diameter (Vegdirektoratet, 2014). This means that the particles will be suspended in water, and the particle-water mix will behave like a viscous fluid where hydrodynamic theory for turbulent flows can be applied.

In a **fully developed debris flow** the volumetric density is higher than for turbulent debris flows. This means that the particles have less free space to move about in, and the debris flow behaves as a continuous flow of particles and water.

A fully developed debris flow can begin by a large and sudden increase in erosion in a river or in a turbulent debris flow. In this case, there is a rapid increase in density and the concentration of solids increases from $C_s = 0.30$ to around $C_s = 0.5-0.7$ (Vegdirektoratet, 2014). This kind of debris flow usually happens in watercourses with easily erodible bottoms, and with a lot of fine-graded material.

Most commonly, fully developed debris flows begins as a smaller initial slide along a drainage path that later erodes masses from the sides of the flow path (Vegdirektoratet, 2014). They can also develop from a landslide. There will be a large variation in the particle size of the debris mass. Fine graded material (diameter < 1 mm) will usually make up about 10-20% of the weight,

while rocks with a diameter of over 10 cm can make up about 50-70% (Vegdirektoratet, 2014).

2.1.2 Triggering Factors and Mechanisms

Predisposing factors for debris flow are steep slopes, loose debris without vegetation and an abundant source of water. Calligaris and Zini (2012) mentions the debris availability as one of the most important predisposing factors, both in the initial release area and also along the run-out path. Areas where long stretches of the run-out path goes across hard rock will be less prone to a debris flow event (Vegdirektoratet, 2014). In an area with an abundant supply of debris, a big precipitation event can be all it takes to trigger a debris flow.

The typical triggering factor of a debris flow is a high intensity precipitation event occurring over a short period of time (Calligaris and Zini, 2012). Other indirect triggering factors can be fires and deforesting. By burning or removing vegetation, the support in the soil is removed. This leads to favorable conditions for a debris flow in an area where there perhaps were no danger before.

Vegdirektoratet (2014) defines two primary triggering mechanisms, the most common one being erosion due to a water flow. The erosion starts when the shear stresses from the water flow exceeds the shear strength of material in the flow path. The content of soil and other debris in the water flow will increase and it can develop into a debris flow. The slope angle have to be higher than 15° for the water flow to reach a sufficient velocity. (Vegdirektoratet, 2014).

A natural drainage path path will in time develop a stronger top layer that will resist erosion (Vegdirektoratet, 2014). This contributes to increased stability in the area. However, change in the climatic conditions can upset this balance, and result in an increased number of debris flow events. Care should be taken when disturbing natural flow paths, e.g. during a road construction project.

Intense rainfall also increases the water saturation and pore pressures, leading to a reduction in the effective stresses in the soil (Kasim et al., 2016). This is the second of the two primary triggering mechanisms in Vegdirektoratet (2014). Here, the pore pressure is the critical factor, not the flow of water on the surface. The permeability of the soil layers have an effect on the

response time (the time before the stability is affected) of increased water supply. Masses with high permeability will fill up quickly, and thus will have a fast response time. Less permeable masses will require e.g. more sustained rainfall in order to fill up and become unstable.

2.1.3 Physics of Debris Flow

Pore pressures higher than hydrostatic pressures are believed to have a significant effect on the run-out distance, by reducing the energy loss along shear surfaces (Laache, 2016). In a series of flume model tests of 10 m³ debris flows, Major and Iverson (1999) found that pore pressures in the flow interiors remained nearly large enough during deceleration and deposition to cause liquefaction. Debris flow deposition was primarily caused by contact friction between grains, and friction with the bed *along the flow perimeter*, where high excess pore pressures are absent. This shows that a reduction in pore pressures will lead to deposition of solids, which in turn will reduce the extent of a debris flow.

The impact force of a debris flow is very difficult to estimate, due to the complex composition of many kinds of sediment sizes and debris. This makes estimating the contact area hard (Kim, 2013). The force from a debris flow can be divided into three stages: First, the impact force when the flow front hits. The front is where large pieces of debris (boulders) accumulate, and is very complex. After the initial impact, the debris flow looks like a mud flow with gradually decreasing discharge. The second stage consists of both dynamic and static forces, while the third stage is only a static force. In total, the debris flow force consists of a hydrostatic force, a hydrodynamic force and the impact force from debris. Of these, the impact force has the most destructive power, and has been the primary interests of many researchers (Kim, 2013). Huebl and Jaeger (2004) conducted full scale impact testing of debris flow, and estimated that the maximum dynamic pressure from the water slurry during a test was 40 kN/m², while impact from boulders could reach 500 kN. Bugnion et al. (2012) reports impact pressures of up to 200 kPa during real-scale experiments.

2.2 Flow Behaviour of Fine-grained Debris Flows

This thesis is focusing on investigating the properties of a fine-grained debris flow, consisting mostly of silt and clay.

For a fine-grained debris flow, the flow behaviour can be defined and investigated through several methods. A key geotechnical parameter is the remoulded shear strength (C_{ur}), although most commonly associated with clay. It gives an indication of a soil's resistance to deformation, and can be measured using the fall cone test. Another parameter that can be used is the quickness value (Q). Originally defined by Thakur and Degago (2012) as a way describing the flow behaviour of sensitive clays, it can also be applied for different soils to give an indication of the flow behaviour. Finally, the viscosity of the soil slurry is an important parameter when characterizing flow behaviour, and is of interest in numerical modeling of debris flows using computational fluid dynamics. It can be measured using a viscometer.

2.2.1 Remoulded Shear Strength

Remoulded shear strength can be used as a measurement of a soil's ability to slide, and is often used in assessment of flow slides in sensitive clays (Adamson, 2017). It can be measured by using the fall cone test.

2.2.2 Quickness

The quickness test follows the concept of the concrete slump test, which is used to measure the consistency of fresh concrete in order to gauge its workability and how easily it flows. To conduct the test, an open cylinder of height H_o is placed on a flat surface and filled with remoulded material. The cylinder is then lifted directly upwards, letting the material flow out. Measurements are taken of the final deformation height H_f and the lateral spread D_f . The quickness value can then be calculated as

$$Q = \left(1 - \frac{H_f}{H_o}\right) \cdot 100\% \quad (2.1)$$

where Q is the quickness value given as a percentage. A quickness value of 0% would indicate total collapse, while a quickness value of 100% would indicate no visible deformation. See figure 2.2 for examples of test results for this kind of test.

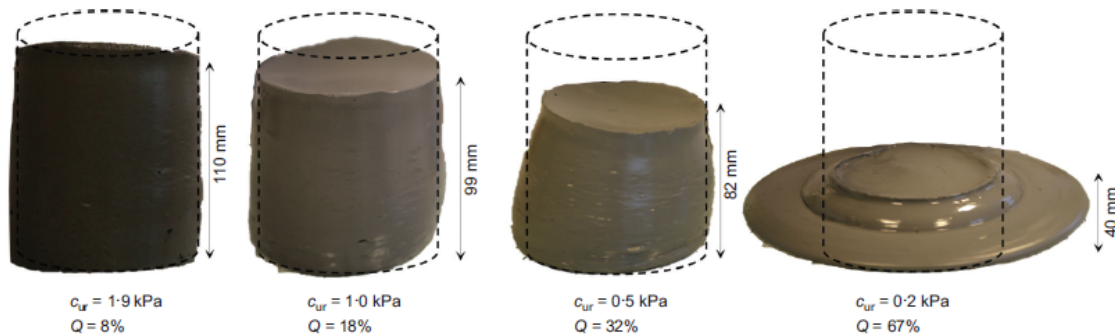


Figure 2.2: Examples on quickness test results on remoulded sensitive clays. Corresponding remoulded shear strength and quickness values (Q) are shown below each test. Figure is taken from Thakur and Degago (2012).

Different cylinder sizes can be used, but Thakur and Degago (2012) recommends a size of 100mm-120mm. This is the size of a Standard Proctor test mold, which is commonly available in most geotechnical laboratories.

In principle, both the undrained shear strength and quickness describes the same soil characteristic through different test procedures. Using the fall cone test to measure the undrained strength of soil in undisturbed and remoulded states gives a point-specific value, while the quickness test provides a value that is representative of the whole volume tested. Additionally, the quickness test has the added value of giving a better visualisation of the flow behaviour of the tested soil (Thakur and Degago, 2012).

Values of $c_{ur} = 1$ kPa and $Q = 15\%$ is proposed as the lower limits for quick clay landslides, based on laboratory testing and back-calculation of Norwegian quick clay landslides (Thakur and Degago, 2012).

2.2.3 Rheology

Rheology is the study of deformation and flow of matter. A key parameter when describing the rheology of a material is the viscosity.

Viscosity

The viscosity of a fluid is the measure of its resistance to deformation due to shear stress or tensile stress. Fluids that obey Newton's linear law of friction are called Newtonian fluids (Irgens, 2014). For a Newtonian fluid in simple shear flow, the shear stress can be expressed as

$$\tau = \mu \cdot \dot{\gamma} \quad (2.2)$$

where τ is the shear stress in Pa, μ is the viscosity in Pa·s and $\dot{\gamma}$ is the shear rate in s⁻¹. For these fluids, the viscosity is equal to a constant value for all shear rates. Water is an example of a Newtonian fluid. Fluids that do not obey Newton's linear law are called non-Newtonian. For non-Newtonian fluids, viscosity is a function of the shear rate, and a viscosity function $\eta(\dot{\gamma})$ is introduced. Equation (2.2) then becomes

$$\tau = \eta(\dot{\gamma}) \cdot \dot{\gamma} \quad (2.3)$$

$\eta(\dot{\gamma})$ is also known as the apparent viscosity (Irgens, 2014). A commonly used model for the viscosity function is given by the power law:

$$\eta(\dot{\gamma}) = K|\dot{\gamma}|^{n-1} \quad (2.4)$$

where K is the consistency parameter in Pa·s ^{n} and n is the dimensionless power law index.

If the viscosity of a fluid is decreasing with increasing shear rate ($n < 1$), the fluid is said to be shear thinning. The opposite, increasing viscosity with increasing shear rates ($n > 1$), is called

shear thickening (Irgens, 2014). Most real non-Newtonian fluids are shear thinning fluids (Irgens, 2014). Figure 2.3 shows examples of flow curves (τ - $\dot{\gamma}$ -curves) for these types of fluids.

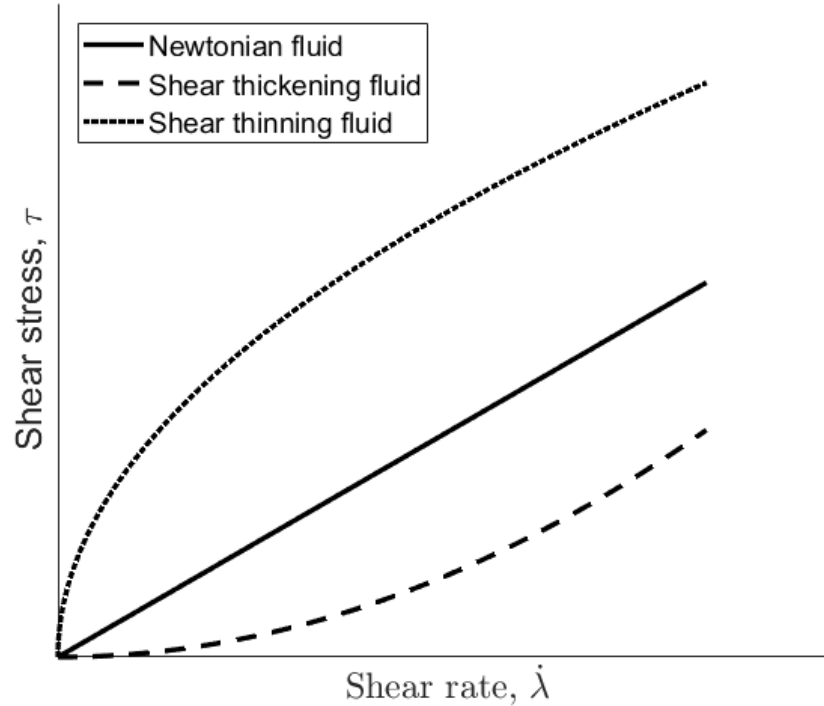


Figure 2.3: Example of flow curves for a Newtonian fluid, and non-Newtonian fluids with shear thinning and shear thickening behaviour.

Viscoplastic fluids are fluids that exhibit a type of yield stress, τ_y . For stresses below the yield stress ($\tau < \tau_y$), the material behaves as an elastic solid. When the stresses exceed the yield stress ($\tau > \tau_y$), the internal network of bindings collapse, and the material behaves as a fluid (Schramm, 1994). The behaviour in the fluid range of shear stresses can be shear thinning, shear thickening or show a linear Newtonian-like flow behaviour. Examples of viscoplastic materials are toothpaste, margarine and fresh concrete (Irgens, 2014).

For certain types of fluids, the viscosity can increase (rheopectic fluids) or decrease (thixotropic fluids) over time. These are called time dependent fluids, and will not be covered here. Refer to Irgens (2014) for more information.

2.2.4 Rheological Models for Fine Grain Rich Debris Flows

Debris Flows with a considerable fraction of fine-grained soil (silt and clay) will in general behave as viscoplastic fluids with shear rate dependent viscosity (Major and Pierson (1992); Kaitna et al. (2007)). Laboratory experiments on suspensions with sandy silt and smaller clay fractions shows shear thinning behaviour (Pellegrino et al.). A characteristic feature of both natural and experimental debris flows is that an apparently unsheared region travels on top of a heavily sheared layer (Kaitna et al., 2007). These observations suggest the idea of a yield stress.

A common non-Newtonian model is the Bingham model. This model was originally proposed for use in debris flow research by Johnson (1970). In the Bingham model, the fluid is given a yield stress τ_B and a constant Bingham viscosity η_B . The model is then expressed as the following linear function:

$$\tau = \tau_B + \eta_B \dot{\gamma} \quad (2.5)$$

The Bingham model describes rheological behaviour well for shear rates $> 20 \text{ s}^{-1}$, however it overestimates the shear stress at lower shear rates (Jeong et al., 2012). This is illustrated in figure 2.4, where it is shown how the stress is overestimated in the lower shear rate region. This can be critical if the model is used to predict a flow where this lower range plays a major role, for example in flow initiation (Coussot and Piau, 1994).

In order to better describe the behaviour for lower shear rates a more general model is needed. In order to also take into account the shear thinning behaviour of water-clay-grain mixtures, the Herschel-Bulkley model has been proposed (Coussot et al., 1998).

2.2.5 Herschel-Bulkley Model

The Herschel-Bulkley model can be seen as a generalized Bingham model (Kaitna et al., 2007). In this model, the shear stress is given as

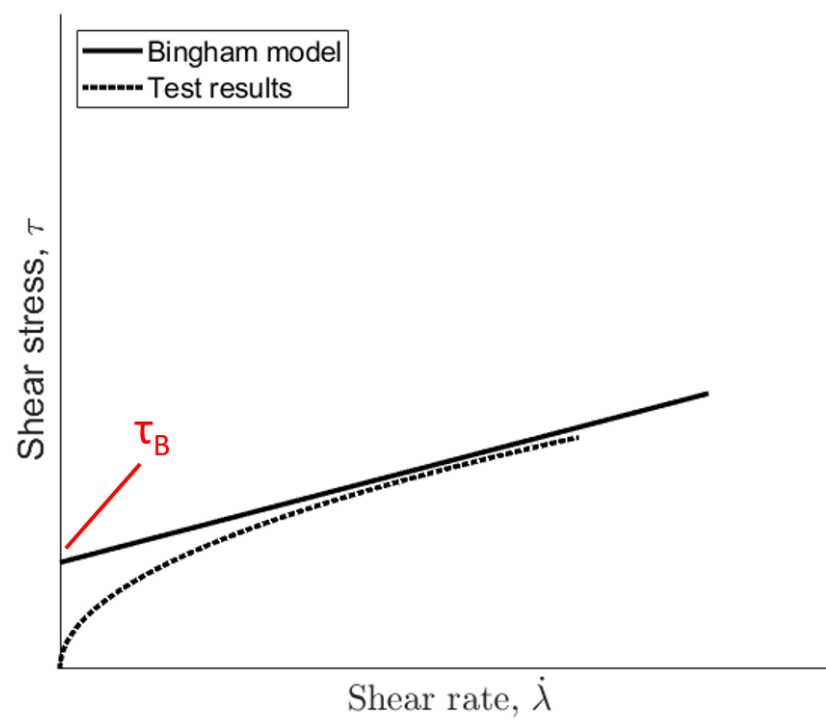


Figure 2.4: Example of how the Bingham model is fitted to experimental data.

$$\tau = \tau_y + K\dot{\gamma}^n \quad (2.6)$$

with τ_y being the yield stress, K a consistency parameter, and n is the Herschel-Bulkley exponent. As for the Bingham model, the yield stress τ_y has to be overcome for the material to flow. For $n < 1$, the model describes shear thinning behaviour, while for $n > 1$ is describing shear thickening behaviour. If $n = 1$ the model becomes the Bingham model. If $n = 0$ and $\tau_y = 0$, it describes a Newtonian fluid.

When fitting the Herschel-Bulkley model to experimental data, the obtained triplet of τ_y , K and n is not unique. Changes to τ_y will lead to large changes in K and n (Coussot and Piau, 1994). Grue (2015) found the final value of τ_y to be a good approximation of the yield stress, but that K and n could vary more.

2.2.6 Viscometry in Debris Flow Research

Rotational viscometers are commonly used in research of debris flow rheology (Pellegrino et al.; Phillips and Davies (1991); Major and Pierson (1992)). Several different rotational rheometers and viscometers exist today, including coaxial cylinder sensor systems, cone-and-plate systems and parallel-plate sensor systems (Schramm, 1994). In this section, the principles behind one type of coaxial cylinder viscometer will be described.

The coaxial cylinder consists of a motor that powers a rotating spindle. The spindle is submerged in a cylinder containing the fluid. A torque detection system measures the torque acting on the rotating spindle as it rotates with constant rotational velocity. Figure 2.5 shows a schematic of the principle behind a coaxial rotational viscometer.

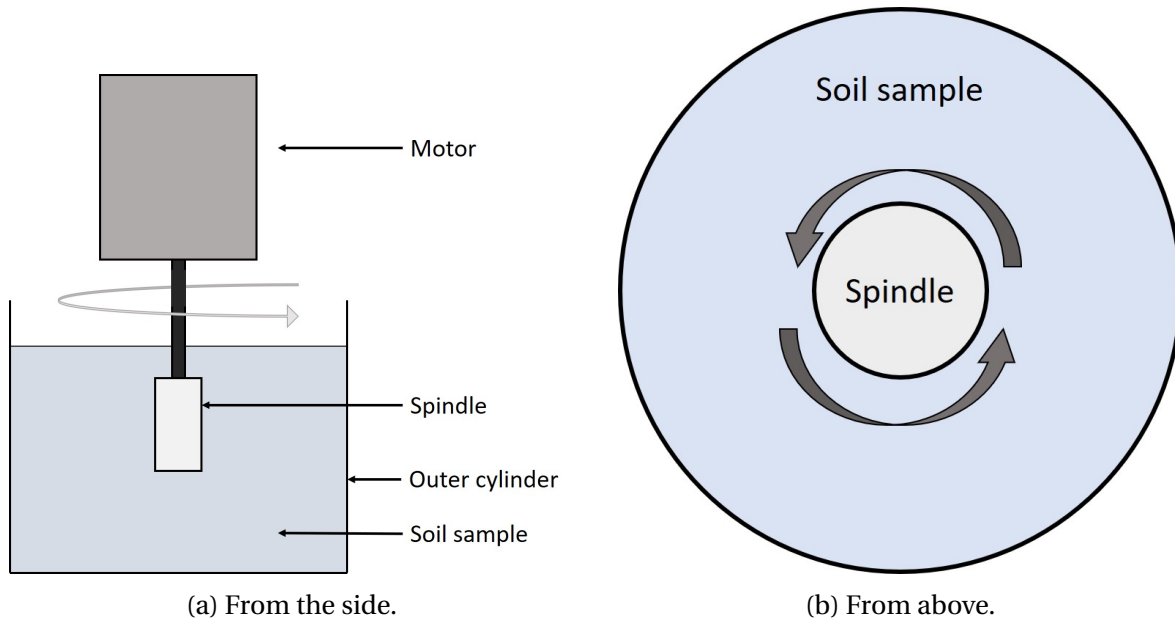


Figure 2.5: Schematic of a coaxial rotational viscometer. The spindle rotates at a certain rotational velocity and measures the torque acting on the spindle.

The velocity profile across the gap between the inner rotating spindle towards the outer, fixed cylinder is non-linear. However, the velocity profile is considered to be approximated well by a simple shear flow with a linear velocity drop if the gap is narrow. The German DIN standards defines a gap as narrow if the ratio between the outer cylinder radius R_o and the inner cylinder (spindle) radius R_i is less than 1.1 (Schramm, 1994). The minimum gap size is dependent on the maximum particle diameter. Schramm (1994) suggest a gap size minimum three times larger than the maximum particle diameter, however a common rule of thumb is ten times larger. The maximum particle size diameter should be less than 1/3 of the gap size (Schramm, 1994). According to Barnes (2000), the gap size should be even larger for $C_s > 25\%$.

The raw data measured in a coaxial rotational viscometer is the torque T (Nm) and rotational velocity N (rotations per second, rps). Certain viscometers are able to display viscosity parameters, but these are derived from the measured torque and velocity, and may not be universally applicable. The derivation of a flow curve $\tau(\dot{\gamma})$ from the torque measurements $T(N)$ is called the *Couette Inverse Problem* (Heirman et al., 2008).

Solution to the *Couette Inverse Problem* for a Wide Gap Viscometer

A straight analytical solution to the *Couette Inverse Problem* for a wide gap viscometer was developed by Heirman et al. (2008). The solution assumes a viscometer in which the outer cylinder rotates, and the inner spindle measures the torque. Solutions were developed for both a Bingham fluid and a Herschel-Bulkley fluid. The primary parts of the Herschel-Bulkley solution will be presented here. For the full derivation of the solution, refer to Heirman et al. (2008).

The shear rate in a rotational flow can be defined as

$$\dot{\gamma}(r) = r \frac{\partial \omega(r)}{\partial r} \quad (2.7)$$

with r being the radial cylindrical coordinate and $\omega(r)$ the angular velocity at radius r . This applies to both narrow and wide gap systems.

According to Heirman et al. (2008), the shear stress of a fluid depends only on the viscometer geometry and not the nature of the fluid. The stress applied to the spindle from the test material is

$$\tau(r) = \frac{T}{2\pi r^2 h} \quad (2.8)$$

where T is the measured torque and h is the height of the spindle. By using equations (2.7) and (2.8) the Herschel-Bulkley formula becomes

$$\frac{T}{2\pi r^2 h} = \tau_y + K \left(r \frac{\partial \omega(r)}{\partial r} \right)^n \quad (2.9)$$

This can be integrated as

$$\int_{R_o}^{R_i} \left(\left(\frac{T}{2\pi r^2 h} - \frac{\tau_y}{K} \right)^{\frac{1}{n}} \frac{1}{r} \right) dr = \int_{\Omega_o}^{\Omega_i} d\omega(r) \quad (2.10)$$

Here, R_i and R_o is the radius of the spindle and the outer cylinder, respectively. $\omega(r)$ is the

angular velocity at radius r . Ω_i and Ω_o is the angular velocity of the flow at the inner and outer boundaries, respectively. Assuming idealistic no slip boundaries conditions, $\Omega_o = 0$ and $\Omega_i = 2\pi$ for a rotational viscometer as shown in 2.5.

This integral can not be solved analytically into a general form when $n \neq 0$. Heirman et al. (2008) developed an expression used to transform the solution into a general form. By dividing the flow behaviour of a material into a flow rate independent constant G_{HB} and a flow dependent component $H_{HB}N^J$. H_{HB} is a viscosity factor and J is a flow index factor. Then the relationship between torque and rotational speed can be expressed by

$$T = G_{HB} + H_{HB}N^J \quad (2.11)$$

where G_{HB} is calculated in Nm, H_{HB} in Nms^J and J is dimensionless. To find the values of G_{HB} , H_{HB} and J , a non-linear least square method can be used. Then the following equations can be used to calculate τ_y , n and K .

$$\tau_y = \frac{G_{HB}}{4\pi h} \left(\frac{1}{R_i^2} - \frac{1}{R_o^2} \right) \frac{1}{\ln(R_o/R_i)} \quad (2.12)$$

$$n = J \quad (2.13)$$

$$K = \frac{H_{HB}}{2^{2n+1}\pi^{n+1}h} n^n \left(\frac{1}{R_i^{2/n}} - \frac{1}{R_o^{2/n}} \right)^n \quad (2.14)$$

2.2.7 Previous Studies On Herschel-Bulkley Parameters for Fine-Grained Debris Flows

Viscometer tests have been used by several authors to find values for Herschel-Bulkley parameters for fine-grained debris flow material.

Major and Pierson (1992) conducted tests in a wide gap rotational viscometer, using debris flow material from a 1980 North Fork Toutle River volcanic debris flow. Tests were conducted for different concentrations (C_s). The material consisted primarily of fine grained particles (clay and silt), sand was added in increasing amounts. Selected results are given in table 2.1.

Table 2.1: Selected Herschel-Bulkley parameters from Major and Pierson (1992). Clay and silt mixed with sand.

C_s	C_s of sand	τ_y	K	n
0.52	0.00	163	11.4	0.9
0.51	0.00	65	51.6	0.4
0.50	0.00	106	16.1	0.4
0.49	0.00	99	6.8	0.4
0.48	0.00	15	25.7	0.3
0.45	0.00	24	2.1	0.4
0.44	0.00	12	2.0	1.5
0.53	0.04	147	15.4	0.9
0.52	0.04	145	0.5	1.3
0.50	0.04	32	16.5	0.3
0.49	0.04	60	0.1	1.5

Viscometer testing on different fine-grained soils was conducted by Adamson (2017). Tests were done on clay, clayey silt and silt, and water was added to vary the remoulded shear strength. The Herschel-Bulkley parameters for some of the tests are given in table 2.2. Only the tests for soil with the lowest remoulded shear strengths (C_{ur}) are presented here. Note that the testing was done at around 7°C in order to represent the in-situ conditions for soil deeper than the surface level. The tests on silt had problems with segregation during testing, and was excluded from further assessment.

Table 2.2: Herschel-Bulkley parameters for different soils. Testing done at ca 7°C. From Adamson (2017). *The silt material had problems with segregation during testing.

Material	C_{ur} [kPa]	τ_y [Pa]	K [Pa]	n [-]
Tiller clay 1	<0.10	90.39	20.54	0.27
Tiller clay 1	0.10	142.41	21.23	0.31
Tiller Clay 2	<0.10	14.31	8.55	0.28
Tiller Clay 2	0.10	65.94	14.37	0.27
Clayey Silt	<0.10	59.06	15.90	0.28
Clayey Silt	0.10	79.23	21.74	0.28
Silt*	<0.10	6.55	0.98	0.73
Silt*	0.10	4.15	1.82	0.66

2.3 Physical Modeling of Debris Flow

It is difficult to obtain detailed measurements of a naturally occurring debris flow. Field data is typically limited by unknown and or irreproducible events and conditions (Iverson et al., 2010). In order to develop models for use in prediction and interpretation of debris flow, detailed data are necessary. Small-scale model testing is a common method of studying debris flows, but it has some limitations when it comes to the effect of scaling.

2.3.1 Small-scale Theory

When doing experiments in a miniaturised model, it is important to consider the effects of scaling. There is some debate on whether or not it is even possible to simulate debris flows in a scale model (Vagnon and Segalini, 2016). Achieving geometric similarity is simple, and is given by the ratio (λ) of a characteristic length (L) of a full-scale (natural) event and a model event:

$$\lambda = \frac{L_{\text{full scale}}}{L_{\text{model}}} \quad (2.15)$$

The challenge comes from achieving full dynamic similarity of all forces, including gravitational and viscous forces. A debris flow can be considered an open channel flow, in which gravitational forces will dominate. This means that the Froude number is the most relevant dimensionless number for scaling. The Froude number can be defined as

$$Fr = \frac{v}{\sqrt{gH}} \quad (2.16)$$

where v is the velocity, g is the gravitational constant and H is the flow height. It is generally thought that results from small scale tests are acceptable if the resulting Froude numbers are comparable with Froude numbers in real events (Hübl et al. (2009); Canelli et al. (2012); Scheidl et al. (2013); Vagnon and Segalini (2016)). Hübl et al. (2009) suggested that the maximum acceptable Froude number in a scale model is 3. Debris flows in nature usually has a velocity in the range of 5–10 m/s, and a flow height of about 1 m (Laache, 2016), giving a range of Froude

numbers equal to 1.60–3.19. However, alpine debris flows are characterized by high velocities (greater than 10 m/s) and shallow flow heights (from 0.2 to 1.5 m) (Vagnon and Segalini, 2016), giving a range of Froude numbers equal to a minimum of 2.61 - 7.14. Major and Iverson (1999) reports that debris flows can travel at velocities of more than 30 m/s, which could lead to even higher Froude numbers.

The equivalent values of a full scale event can be estimated from the results of a miniaturised test using the ratio (λ) from equation (2.15). Velocities (v) can be estimated as

$$v_{\text{full scale}} = \sqrt{\lambda} \cdot v_{\text{model}} \quad (2.17)$$

while forces (F) and pressures (p) can be estimated as

$$F_{\text{full scale}} = \lambda^3 \cdot F_{\text{model}} \quad (2.18)$$

and

$$p_{\text{full scale}} = \lambda \cdot p_{\text{model}} \quad (2.19)$$

2.4 Analytical Models for estimating Debris Flow Impact Forces

For the purpose of analytically estimating the impact forces of a debris flow, different models have been developed. As models based only on theoretical considerations are not able to estimate the impact pressure with sufficient accuracy or acceptable computation time, empirical models based on observations and theory have been developed and used (Proske et al., 2011).

Different types of debris flow impact models exist, and two classes of models are the hydraulic and solid body collision models (Hübl et al., 2009). Solid body collision models covers the impact from larger pieces of solid debris, while the hydraulic models are related to the impact thrust of the fluid-phase slurry (Scheidl et al., 2013). For the work in this thesis, the hydraulic

models are the most relevant.

Hydraulic models are popular and relates impact pressures to the hydrostatic pressure, hydrodynamic pressure or a mix of both (Vagnon and Segalini, 2016). The hydrostatic model was formulated by Liechtenhahn (1977) as:

$$F_{\max} = k \cdot \rho_m \cdot g \cdot h_f \cdot A \quad (2.20)$$

where F_{\max} is the maximum force during the impact in N, k is an empirical coefficient, ρ_m is the mean bulk density of the impacting flow volume in kgm^{-3} , g is the gravitational acceleration in m s^{-2} , h_f is the flow height and A is the impact surface in m^2 . This formula is popular for use in engineering design, because the only unknown parameter is the debris flow height. By using the height of the impacted structure as the flow height, all parameters will be known. The empirical k factor takes into account the dynamic flow component and behaviour of the flow, and can assume values ranging from 2.5 to 11 (Armanini and Michiue (1997), Scotton and Deganutti (1997), Liechtenhahn (1977)).

The hydrodynamic models are based on the impulse theorem (Proske et al., 2011) and the hypothesis that the flow is a homogeneous fluid. For an impassable obstacle, the model can be expressed as

$$F_{\max} = a \cdot \rho_m \cdot v_f^2 \cdot A \quad (2.21)$$

where a is a dynamic coefficient and v_f is the flow velocity upon impact. The coefficient a is the key part in this equation, and is an empirical factor that takes into account the obstacle and debris flow characteristics. It is inversely correlated with the the drainage capability of the impacted object, due to discharge of fluid through the object. The grain size distribution of the debris flow will also have an effect, with coarser distributions increasing the value of the coefficient due to local overpressure build up from impacting boulders (Vagnon and Segalini, 2016).

A wide range of values for the coefficient a is reported in the scientific literature. Hungr et al.

(1984) proposes a value of 1.5, Daido (1993) proposes a range of 5 to 12, Zhang (1993) suggest between 3 and 5, Bugnion et al. (2012) from 0.4 to 0.8, and Canelli et al. (2012) gives between 1.5 and 5. The values reported range from 0.4 to 12, making it clear that the impact force depends greatly on the flow conditions and the characteristics of the impacted object (Vagnon and Segalini, 2016).

A relation between the hydrostatic coefficient k and the hydrodynamic coefficient a can be based on the Bernoulli energy line:

$$k \cdot \rho_m \cdot g \cdot h = a \cdot \rho_m \cdot \frac{v^2}{2} \quad (2.22)$$

Proske et al. (2011) collected data from both miniaturised tests and full scale tests in order to compare the hydraulic models. The measured impact pressures were normalised by pressure from hydrostatic and hydrodynamic formulas, and then plotted with Froude numbers. It was shown that the hydrostatic formulas performed best for low Froude numbers, while the hydrodynamic formulas performed best for the higher Froude numbers. A higher Froude number is related to a higher velocity, and thus the hydrodynamic part of the impact force is increasing with Froude number (given that the flow height is not increased).

Chapter 3

Laboratory Experiments

This chapter outlines and describes the laboratory experiments undertaken as part of research on debris flows. The purpose was to test the behaviour and characteristics of a muddy, fine-rich viscous type of debris flow. The focus was put on this type of flow partly because the laboratory results were thought to be more fit for later use in a research project into numerical modeling of debris flows, using computational fluid dynamics (CFD). Apart from the initial index tests of the soil material that was going to be used, this chapter consists of two parts. The first part details the tests associated with flow behaviour of the material at different concentrations. The second part is dedicated to model testing conducted in a flume model.

3.1 Test Material

The purpose of the test program was to study a viscous type of debris flow that would not segregate during testing. It was decided to use a waste material from the washing process of sand and gravel from a quarry in Stokke. This soil was a silt material with grain sizes below 0.125 mm. Originally, the plan was to use only one type of soil. However, the material was procured in two batches, and it was discovered during testing that the grain size distribution varied between them. In particular, the clay content of the second batch was about twice as high as the first batch. The soil from the first and second batch will be referred to as soil 1 and soil 2, respec-

tively.

3.1.1 Grain Size Distribution

The grain size distribution was found by conducting a hydrometer test on the material. The method is described in the guideline by Vegdirektoratet (2016). Two tests were conducted on each material, and the averaged grain size distributions are shown in figure 3.1. As seen, the major difference between soils 1 and 2 is the clay content. The clay content is approximately 6% in soil 1 and approximately 11% in soil 2.

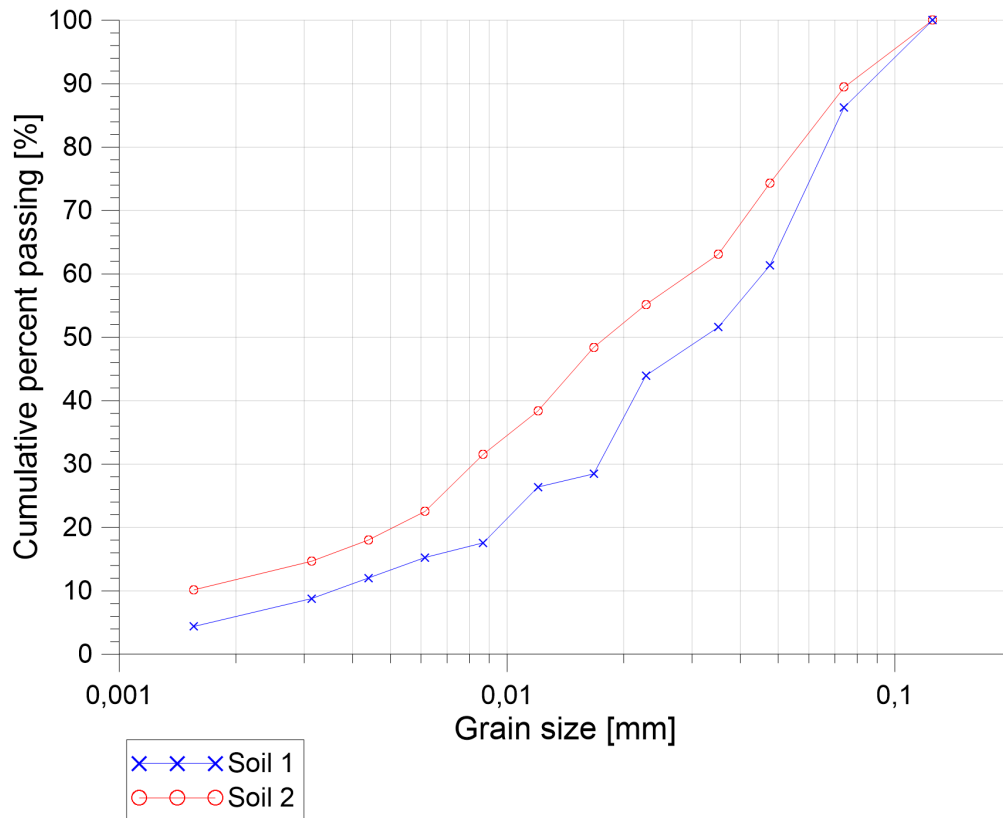


Figure 3.1: Grain size distribution curves for soil 1 and soil 2.

3.1.2 Dry Density

The dry density of the soil used were found by conducting pycnometer tests in accordance with the guideline from Vegdirektoratet (2016). The dry density was found to be 2.79 g/cm^3 for soil 1,

and 2.86 g/cm^3 for soil 2.

3.2 Flow Behaviour Testing

To quantify the flow behaviour of the debris flow material, three different parameters were investigated: remoulded shear strength, quickness value and viscosity. The remoulded shear strength was found using the fall cone test. The quickness value was found using the quickness test. A rotational viscometer was used to find the viscosity. The remoulded shear strength and quickness describes the ability to flow, and these values are also used when selecting material concentrations for flume model testing. The viscosity describes how the material will flow, and is an important parameter in numerical modeling.

The study of the flow behaviour was done for different concentrations of solids. The concentration of solids (C_s) is here defined as:

$$C_s = \frac{\text{Volume of dry soil}}{\text{Volume of dry soil} + \text{Volume of water}} \quad (3.1)$$

The test program consisted of testing of the remoulded shear strength, quickness and viscosity for different values of C_s for the two soils. Soil 1 was used as the primary material, while soil 2 was used to test the effect of altering the clay content. Table 3.1 shows a list of the different solid concentrations (C_s) and which soil was used for the flow behaviour tests.

Table 3.1: Table of solid concentrations used for flow behaviour tests (remoulded shear strength, quickness and viscosity)

Test number	Test name	Soil	Concentration of solids [%]
1	C30S1	1	30
2	C35S1	1	35
3	C40S1	1	40
4	C45S1	1	45
5	C20S2	2	20
6	C30S2	2	30

3.2.1 Sample Preparation

The soil was stored covered in plastic in buckets and a wooden crate in the laboratory. The water content was checked before each day of testing. Before conducting the tests, the amount of soil and water needed to achieve the desired C_s was added to a plastic bowl. A stand mixer with a dough hook was used to mix the material into a homogenized slurry. The tests were carried out as soon as possible after the mixing was stopped, in order to minimize segregation of the material.

3.2.2 Remoulded Shear Strength

The remoulded shear strength was tested using the fall cone test. The cone types used were 10 g, 60° cones. The procedure was in accordance with the method described in Handbook R210 by Vegdirektoratet (2016). The indentation was recorded and converted to shear strength using the conversion tables. Each sample was tested 2 times without remoulding in between. It was then remoulded and tested 2 times more, making for a total of 4 indentations. The average was used to find the shear strength.

3.2.3 Quickness Test

The quickness of the material was determined using the method mentioned previously. A Standard Proctor mold (height 102 mm, diameter: 116 mm, volume: 1078 cm³) was coated with a thin layer of oil on the inside to provide a non-stick surface.

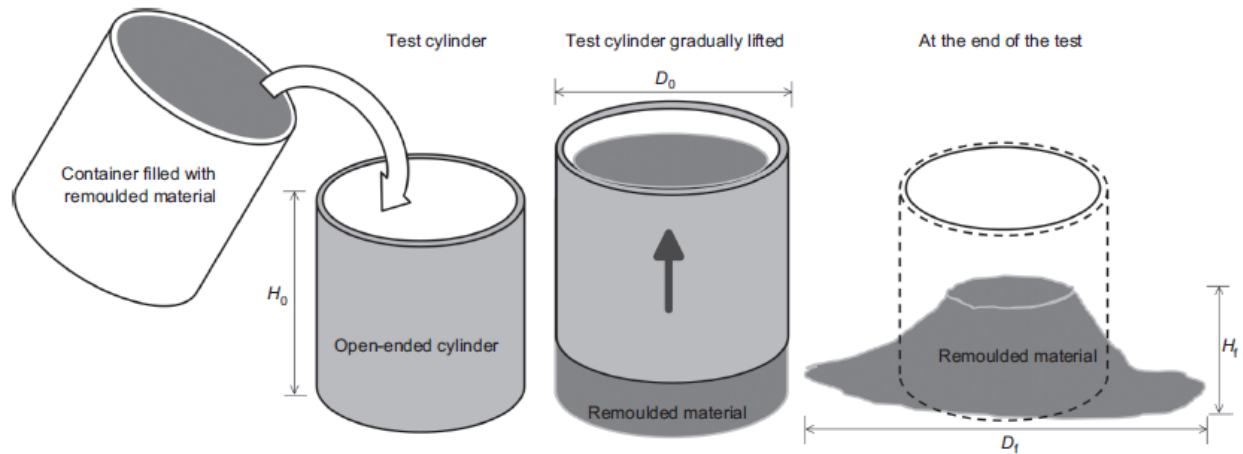


Figure 3.2: Quickness test procedure, taken from Thakur and Degago (2012)

The mold was placed on a clean, flat plastic surface and filled to the top with remixed material. The surface was levelled using a thin blade, before the mold was lifted in a smooth fluid motion. See figures 3.3a and 3.3b for an example test. The method is illustrated in figure 3.2..



(a) Before



(b) After

Figure 3.3: Picture of the before and after a quickness test. The test in the photograph is an example test and not part of the test program.

The test was finished as soon as the material stopped moving (usually less than a second after lifting the mold). A measurement of the deformation height was taken by inserting a thin ruler into the middle of the sample. The lateral spread was measured using a folding ruler. The

quickness value was then calculated using equation (2.1).

3.2.4 Viscometer Test

A coaxial rotational viscometer was used to determine the rheological behaviour for different concentrations of the fine-grained soil.

Instrument

The viscometer used was a Bohlin Visco 88 BV. A rotating spindle is covered by an outer cylinder. Different spindle and cylinder diameters were available, but only one combination was used. The viscometers features 8 speed settings, ranging geometrically from 20–1000 RPM. The outer cylinder was fixed without any rotation.

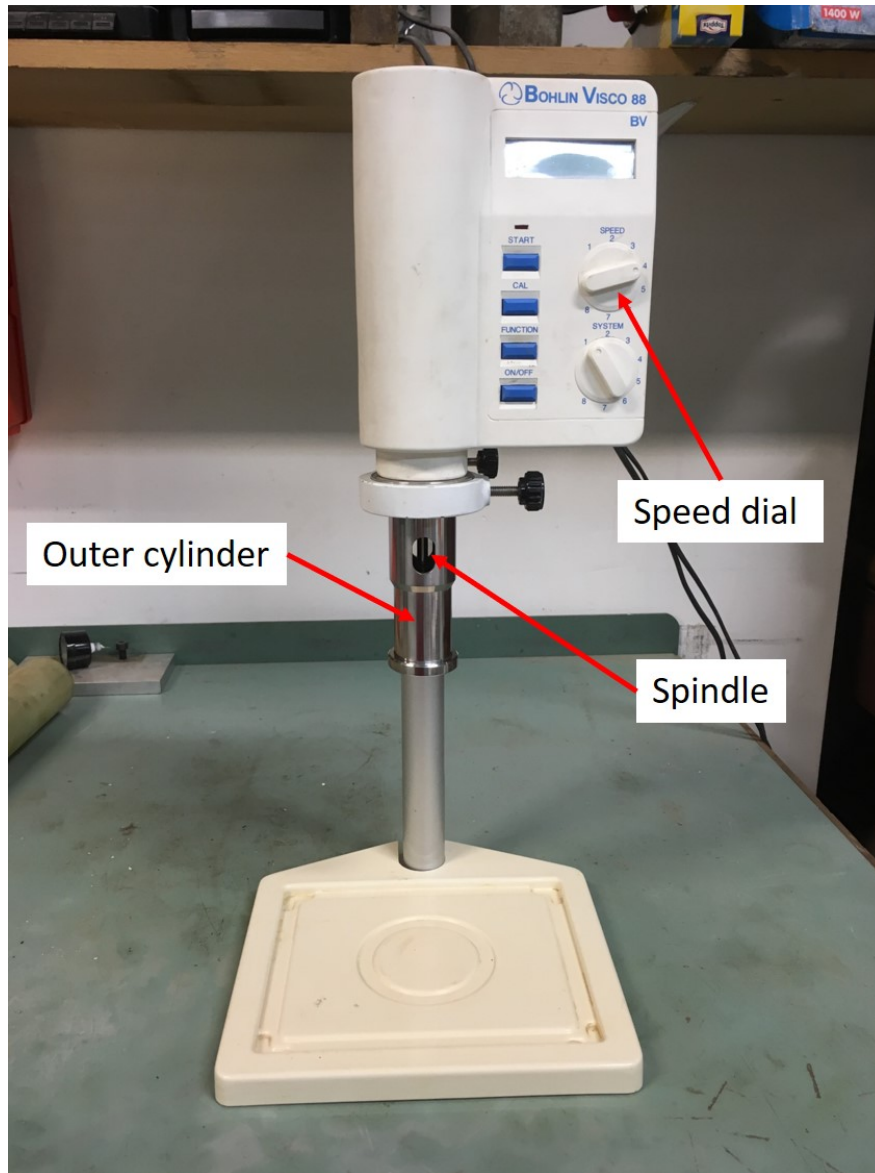


Figure 3.4: Bohlin Visco 88 BV Viscometer

The instrument measures torque (mNm), rotations per second (Hz) and temperature ($^{\circ}\text{C}$). Viscosity, shear rate and shear stress could also be displayed, however these are calculated for Newtonian fluids. The material tested is assumed to show non-Newtonian behaviour. Only torque, rotations per second and temperature was recorded.

Table 3.2: Speed settings on the Bohlin Visco 88 BV

Speed setting	Rotational Speed, N [Hz]	Angular Velocity, ω [rad s ⁻¹]
1	0.33	2.09
2	0.58	3.67
3	1.02	6.39
4	1.78	11.21
5	3.12	19.58
6	5.45	34.24
7	9.53	59.90
8	16.67	104.72

A wide-gap system was used to avoid problems with the gap being too small compared to the maximum grain size in the material. Table 3.3 lists the dimensions of the cylinder and spindle used, in addition to the gap ratio R_o/R_i

Table 3.3: Dimensions of the viscometer spindle and cylinder pair used in the experiments.

Spindle radius, R_i [mm]	Height, h [mm]	R_o [mm]	R_o/R_i [-]
7.0	21.1	13.75	1.96

The test procedure is based on the precedent set by Grue (2015) and Adamson (2017). It consists of finding an equilibrium torque before starting the dynamic response test.

Finding the Equilibrium Torque

As soon as the mixing procedure was finished, the material was poured into the outer cylinder. The cylinder was then locked in place and the viscometer was started. The material sample was sheared until an equilibrium torque value was obtained. To obtain the equilibrium torque, different rotational speeds was applied for 2 minutes each, each time with the highest speed (speed 8) for 2 minutes in between. The equilibrium torque was chosen as the lowest recorded value that was possible to achieve every time the speed was changed from a lower speed to the

highest speed. This value was used as the start value for every new rotational speed in the dynamic test.

Dynamic Response Test

After the equilibrium torque value was found, the dynamic response test was started. The procedure was to shear the sample at the highest speed until equilibrium torque was reached, before reducing stepwise reducing the speed. The sample was then sheared at the lower speed for 2 minutes. Before going to the next lower velocity, the sample was sheared at speed 8 until it achieved equilibrium torque. The sequence then became (8, 7, 8, 6, 8, 5, ... et cetera).

A video camera was used to record the display during the dynamic response test, and a stopwatch was used to keep track of the time elapsed. Measurements of the torque was taken at 0 s, 5 s, 10 s, 15 s, 20 s, 30 s, 40 s, 60 s and 120 s for each speed setting. The measurements was started as soon as value was displayed. Temperature and rotational speed was taken after 60 s.

The torque value measured after 15 s was used to create a $T(N)$ plot, each plot consisting of 7 points (the highest speed was excluded).

Basic Assumptions

The basic assumptions for measuring viscosity by using a rotational viscometer are (Schramm, 1994):

- Laminar flow.
- Steady state flow.
- No slippage at boundaries.
- Samples must be homogeneous.

Turbulence in the flow can be detected when the equilibrium torque value is much higher than the torque at lower speed (Grue, 2015). The reason is that a much higher torque value is needed to maintain turbulent flow.

The torque measurement used for for the $T(N)$ plot should be representative for steady state conditions. To ensure this, the torque measurement was taken after 15 seconds, as this was assumed to be enough time to attain a constant value.

No slip conditions are assumed at the boundary wall. Zero velocity was assumed at the outer cylinder wall. At the spindle boundary, the flow velocity was assumed to be equal to the angular velocity of the spindle.

3.3 Flume model testing

This section covers the tests conducted in a flume model located at the Norwegian University for Science and Technology (NTNU). A core set of six tests were conducted, testing variations in flow volume and concentration of solids (C_s) using the same soil for all but one test. The variation in grain size distribution for the two soil batches was not discovered before testing had begun. The amount of material in the first batch (soil 1) was only enough to cover five of the six six tests. The final test was done using the soil from the second batch (soil 2). Additional tests were done in order to study the effect of changing the material. In total, 22 test repetitions were completed.

3.3.1 Flume Model at NTNU

The debris flow model used for this study is a general model with a scale of 1:20. It is not meant to model a specific event, but a general debris flow. It is a completely new model as of 2018, but the design is based on a previous model that was built in 2009 and used in several different works, including Hiller and Jenssen (2009), Fiskum (2012), Christiansen (2013), Laache (2016) and Yifru et al. (2017).

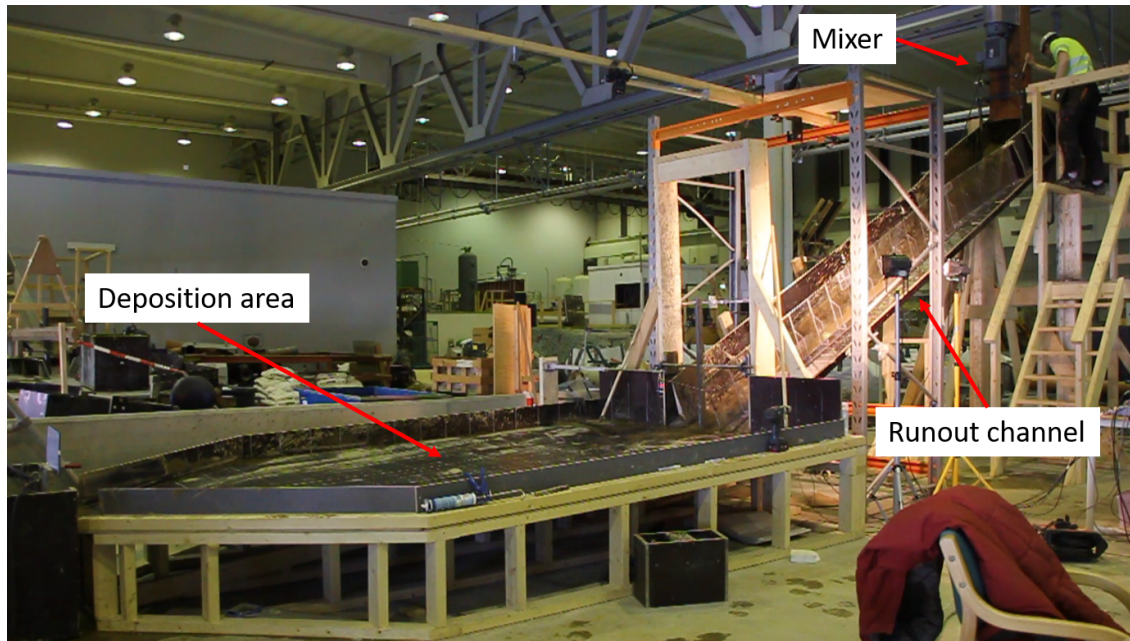


Figure 3.5: Picture of the flume model at NTNU.

The new flume model consists of an angled runout path and a slightly angled deposition plate area. Special features include the ability to alter the slope angle and channel width, and a transparent wall in the runout area. The runout channel is 5 m long, while the deposition area is 4 m long. For this study, the runout channel width was set to 0.3 m and the slope angle was set to 27° . See figure 3.6 for a picture of the runout channel.

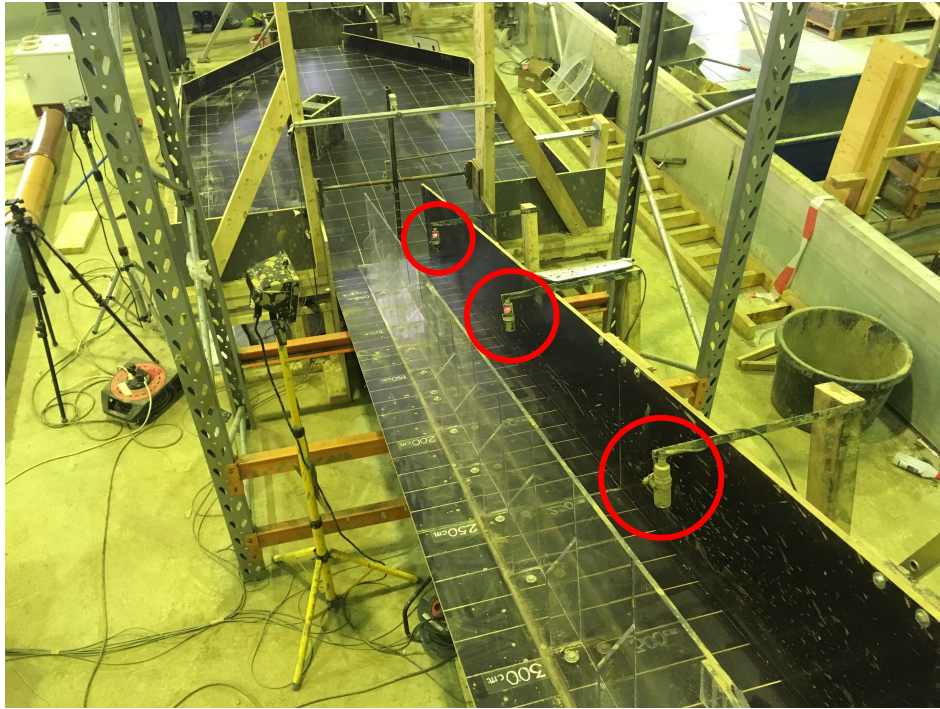


Figure 3.6: The runout channel. Flow height sensors are circled.)

For the release of the flow material, an automatic mixer was built. The mixer consists of a metal cylinder with a width of 0.39 m and height of 1.55 m, with an electrical motor welded to the side, powering a mixer on the inside. On the bottom there is a hatch which opens at the pull of a lever. The weight is about 230 kg and requires the use of a crane to be lifted in place. See figure 3.7 for a picture of the mixer.

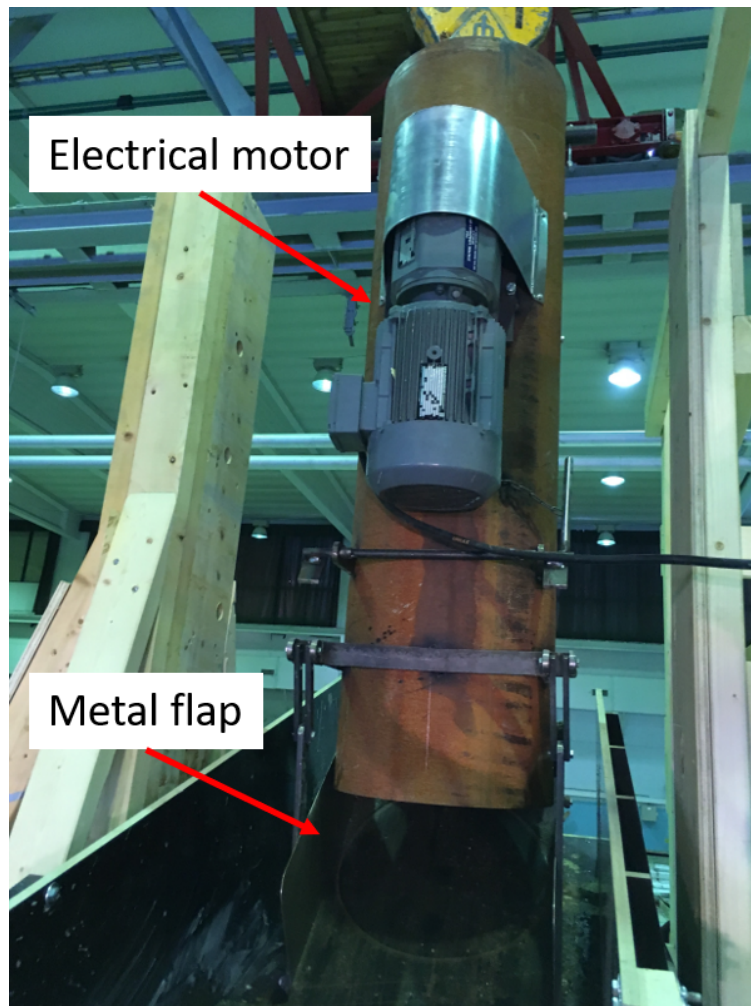


Figure 3.7: The mixer used to mix and release the debris flow material.)

3.3.2 Instrumentation

The instrumentation in the flume model consisted of cameras, flow heights sensors, pore pressure sensors and a metal pillar connected to a force sensors. Figure 3.8 shows a drawing of the model and the placement of instrumentation.

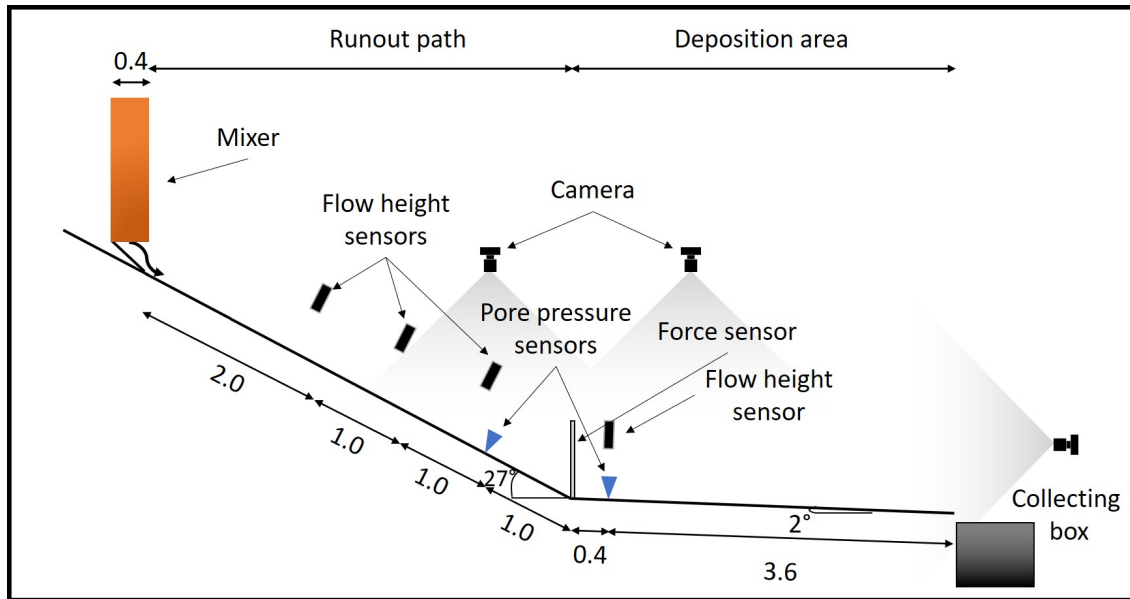
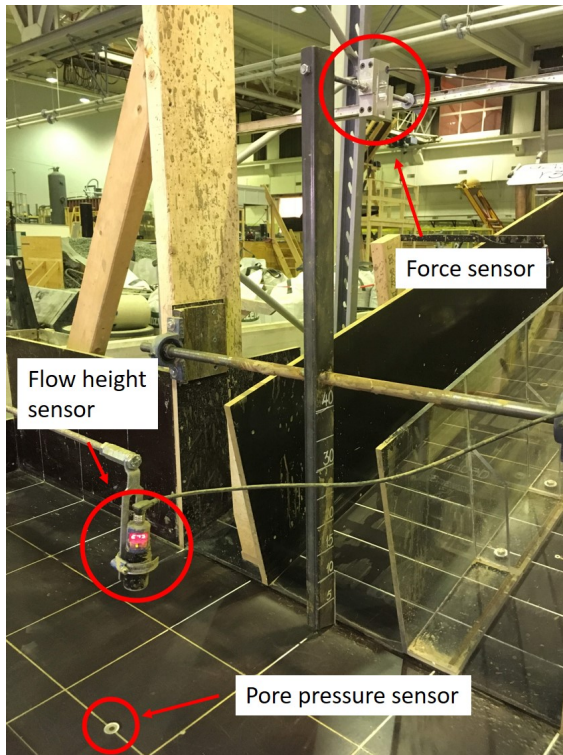


Figure 3.8: Sketch of the flume model with instrumentation (all linear dimensions are in meters)

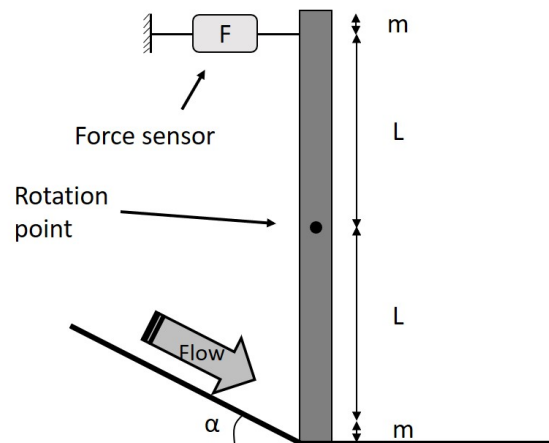
Different cameras were used throughout the test program, but three general locations were used. The first location was above the runout channel. Cameras mounted in this position were capable of recording at high frame rates (120 frames per second and upwards), and were primarily used to measure the velocity of the flow. In a select few tests, a Phantom VEO 410L high-speed camera was used to record video at 1000 frames per second. This made it possible to study the flow behaviour and the interaction between the flow and the metal pillar with force sensor. The second camera was positioned above the deposition area, and made it possible to study the deposition process. The third camera position was facing the entire model from the far end of the deposition area, having an overview of the entire model.

A total of four ultrasonic flow height sensors were installed. The first three were placed 3, 2 and 1 m before the end of the runout channel, while the fourth was placed 0.4 m after the beginning of the deposition area. These measured the flow height directly below them during the duration of a test. The data was logged to a computer at a rate of 50 Hz, and the logging was activated by a foot switch.

Two pore pressure sensors were installed underneath the final two flow height sensors, 1 m before and 0.4 m after the end of the runout channel. These measured the pore pressure in millimeter water column (mmwc) at a rate of 50 Hz, and was also activated by the foot switch.



(a) Picture of the force sensor. The metal pillar is impacted at the bottom, and the force sensor registers the force.



(b) Drawing of the force sensor. In the test setup used in this work, $L = 440$ mm and $m = 15$ mm. The width is 25 mm.

For measuring the impact force of the debris flow, a rectangular metal pillar mounted on axle was used. The rod was able to rotate freely parallel to the flow on frictionless bearings. A load cell installed at the top of the metal pillar measured the force acting on the opposite, lower end. This made it possible to measure the impact force of the debris flow under the assumption that the resultant force was hitting the exact same point as the force sensor, only on the opposite end. The force sensor was connected to the computer logger, and was also activated by the foot switch, recording the force at a rate of 50 Hz. See figure 3.9a for a picture of the force sensor.

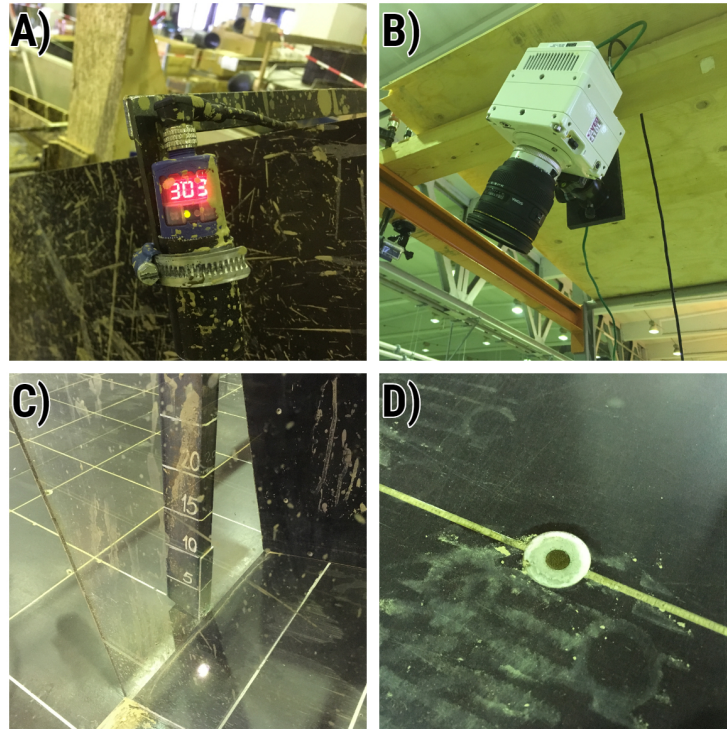


Figure 3.10: A) Flow height sensor. B) Phantom VEO 410L High-speed camera. C) Impact area of force sensor. D) Pore pressure sensor.

Figure 3.10 shows pictures of some of the instrumentation.

3.3.3 Expected Range of Results

The physical model was made to a scale of approximately 1:20. In accordance with the small-scale theory mentioned previously, scaling by Froude number was assumed to be applicable. This meant that a velocity of 10–15 m/s and flow height of 0.2 m – 1.5 m (Vagnon and Segalini, 2016) would translate to a velocity of over 2.24–3.35 m/s and flow heights of 0.001 – 0.075 m in the model. A maximum dynamic water pressure of 40 kPa would translate to a pressure of 2 kPa ((Proske et al.), while a maximum impact pressure of 200 kPa would translate to a pressure of 10 kPa in the model.

3.3.4 Test plan

Based on the experiences from the testing of the flow behaviour, it was decided to test three different concentrations (C_s of 35%, 40% and 45%) and two different volumes (40 L and 20 L) in the flume model. This makes for a total of six test sets. The concentrations were decided based on the expectation that the modeled debris flow would be able to reach the deposition area without stopping. The slope angle was set to 27° for this reason as well.

As mentioned previously, there was only enough of soil 1 to complete five of the six test sets. For the sixth test (which was supposed to be C_s 35%, 20 L), soil 2 had to be used. It was decided to use a concentration with a similar quickness value as soil 1 with $C_s = 35\%$. Hypothetically, viscosity data could also have been used, but due to limited time, the quickness value was used instead. The hypothesis was that tests using material of the same quickness would give similar results. But it was also believed that altering the grain size distribution could have an effect on the results even if the quickness values were the same. To check this, additional tests were carried out using soil 2 and with a quickness value similar to soil 1 with a $C_s = 45\%$.

Table 3.4: Test plan for the flume model testing. Test set 7 and 8 consists of only one repetition each.

Test set	Test name	C_s [%]	Quickness [%]	Volume [L]	Soil number	Comment
1	Q93S1V40	35	93	40	1	
2	Q95S2V20	20	95	20	2	Quickness similar to soil 1 with C_s 35%
3	Q85S1V40	40	85	40	1	
4	Q85S1V20	40	85	20	1	
5	Q77S1V40	45	77	40	1	High-speed camera (1000 FPS)
6	Q77S1V20	45	77	20	1	High-speed camera (1000 FPS)
7	Q77S2V40	30	77	40	2	Quickness similar to soil 1 with C_s 45% High-speed camera (1000 FPS)
8	Q77S2V20	30	77	20	2	Quickness similar to soil 1 with C_s 45% High-speed camera (1000 FPS)

The test plan for the flume model testing is shown in table 3.4. In total, eight test sets were carried out, and with the exception of test 7 and test 8, each of the test sets contained three repetitions. The test names given include the quickness value for the solid concentration used (Q77 means a quickness value of 77%), the soil number (1 or 2), and the total volume (40 L or 20 L). Additionally, a number might be added to end when referring to a specific repetition, e.g. Q93S2V40-2 refers to a test with concentration having a quickness value of 93%, soil number 2, a total volume of 40 L and the second repetition.

Test set 1–6 constitutes the core test sets, designed to study the effect of variations in concentration of solids, quickness and flow volume. Test set 7 and 8 were designed to test the effect of using the soil with a higher clay content (soil 2) at similar quickness values.

Test sets 5–8 were also recorded using the high-speed camera (recording at 1000 frames per second) for the purpose of studying flow behaviour and interaction. This camera was only available

for these select tests.

3.3.5 Test procedure

One test repetition takes about 1.5–2.5 hours to complete, depending on whether the test is conducted by one or two persons, and if the material is reused between repetitions or not. The natural water content of the soil being used must be measured in advance.

1. Fill the cylinder with the correct amount soil and water mix to achieve the desired concentration and volume. If reusing material collected from previous test, add more soil and water if necessary.
2. Use a crane to lift the mixer containing the soil-water mix to the release area of the model.
3. Start the mixer, and let the material mix for as long as it takes to achieve a uniform and fluidized mix (about 10-15 minutes).
4. Spray water in the flume channel and deposition area, to ensure the same test conditions every time.
5. Prepare the logging software on the computer.
6. When the material is properly mixed, start the cameras.
7. Activate the computer logger by the foot switch and then open the mixer, releasing the material.
8. Test is finished when the flow stops moving in both the runout channel and deposition area.
9. Stop the cameras, photograph and take the necessary notes of the test results. Fill a container of known volume and weight, and weigh it for checking the post test concentration
10. Clean the model. If another test of the same concentration will be conducted, refill the cylinder with the collected material, adding a measured amount of water and soil if needed. If not, throw the collected material away, and add a measured amount of soil and water in the cylinder for the next intended volume and concentration.

Chapter 4

Processing of Test Data

This chapter outlines and describes the processing of the raw data collected from the viscometer test and the flume model tests. It also covers the calculation of parameters for the analytical debris flow impact force formulas.

4.1 Viscometer data processing

Data from the viscometer test includes torque values T corresponding to different speed settings N , as well as temperature readings. The torque was measured in mNm, but converted to Nm before the processing of data.

The rheology of the test material was assumed to fit the Herschel-Bulkley model. To calculate the values of τ_y , n and K from the T - N data, the previously mentioned method developed by Heirman et al. (2008) was applied. This method have previously been used to process data from the exact same viscometer as used in this thesis by Grue (2015) and Adamson (2017). However, this method was originally developed for a viscometer where the outer cylinder was rotating, while torque was measured on the inner spindle. This has an effect on the velocity distribution (see figure 4.1).

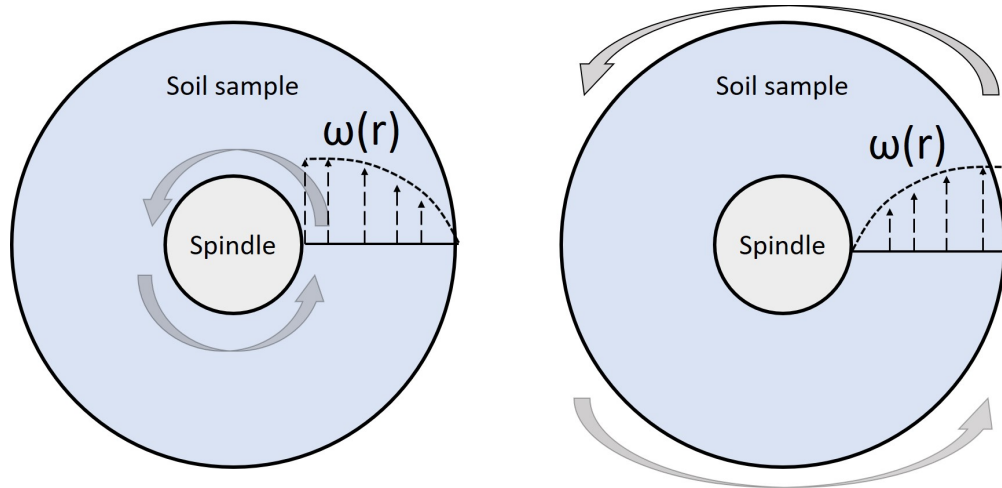


Figure 4.1: Two different rotational viscometer design principles. Left: Inner spindle rotates with angular velocity ω . Right: Outer cylinder rotates with angular velocity ω . The drawn velocity profile is only an illustration of non-linear velocity profile.

To avoid negative term on the right side of the integral in equation (2.10), absolute signs were added. The integral then became:

$$\left| \int_{R_o}^{R_i} \left(\left(\frac{T}{2\pi r^2 h} - \frac{\tau_y}{K} \right)^{\frac{1}{n}} \frac{1}{r} \right) dr \right| = \left| \int_{\Omega_o}^{\Omega_i} d\omega(r) \right| \quad (4.1)$$

It was assumed that this makes the formulas for τ_y , n and K from Heirman et al. (2008) applicable also in this case. However, due to limited time and the complicated nature of the solution to the integral, this was not investigated further.

The recorded data for T and N was fitted to a curve with equation

$$T = aN^b + C \quad (4.2)$$

where $a = H_{HB}$, $b = J$ and $c = G_{HB}$. From this, the values for τ_y , n and K could be calculated using the formulas from Heirman et al. (2008), mentioned previously.

The curve fitting was conducted using MATLAB and the *fit* function from the Curve Fitting Toolbox. The fit function used was a *power2* fit. Based on precedent set by Grue (2015) and Adamson (2017), six different fits were performed for each test:

- Fit 1: All eight points.
- Fit 2: The six last points (point at lowest speed setting excluded).
- Fit 3: The six first points (point at highest speed setting excluded).
- Fit 4: The five first points (points at the two highest speed settings excluded).
- Fit 5: The five middle points (Points at lowest and highest speed settings excluded).
- Fit 6: The three middle points (Points at two highest and two lowest speed settings excluded).

In cases where all of the coefficients a , b and c became negative, new curve fits were made with the added constraint of no negative coefficients.

4.2 Flume Model Test Data

The test data from the flume model tests included video recordings and recorded data from the flow height sensors, pore pressure sensors and the force sensor.

4.2.1 Video Analysis

The video recordings were primarily used for calculation of flow front velocities. The tracking software Tracker Video Analysis and Modeling tool for Physics Education V4.11.0 (<https://physlets.org/tracker/>) was used. It is a simple tool that allows the tracking of an object in a video. By entering a correct reference scale and by tracking the object correctly, data related to the movement of an object is calculated and given as output, including velocity. By tracking the flow front in the videos, the flow front velocity was found.

There were mainly two limitations of this technique. The first was barrel distortion of the image (see figure 4.2). This occurs when the field of view of the lens is wider than the size of the image sensor (Mansurov, 2018). As a result, straight lines are curved inwards. This leads to inaccuracy

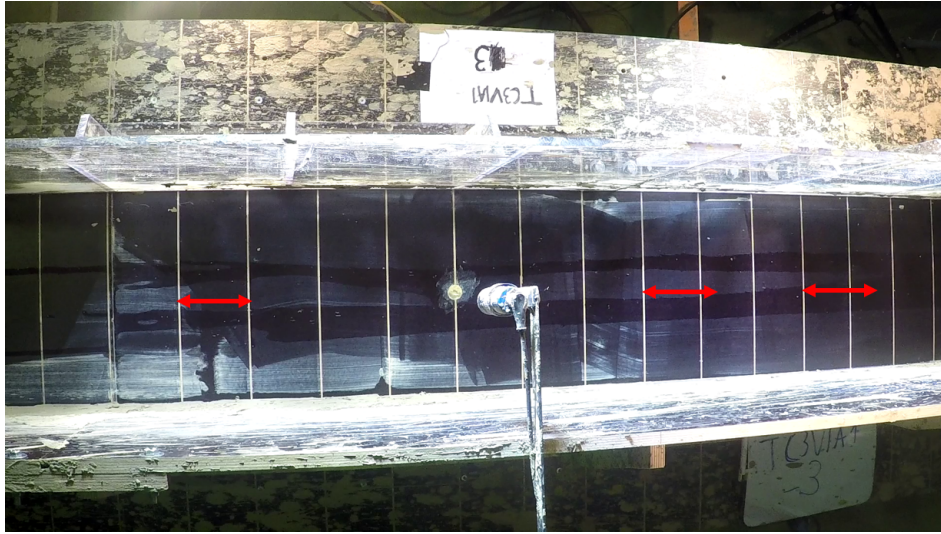
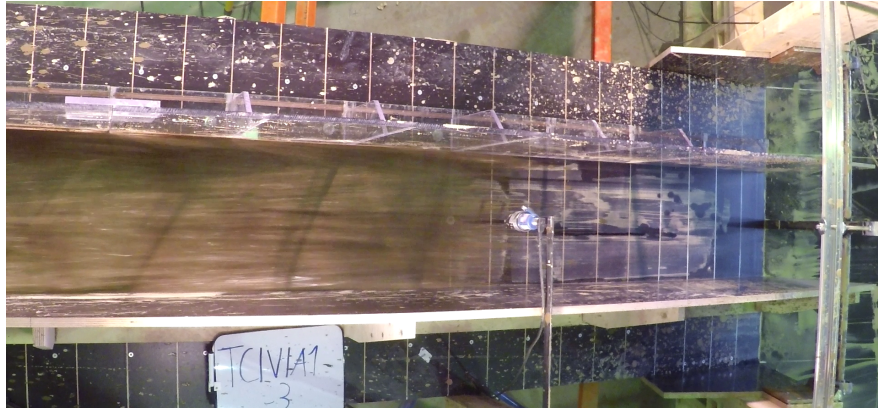


Figure 4.2: Effect of barrel distortion illustrated. The red arrows are equal in length, in reality the distance between each of the white stripes is 10 cm.

in the calculated velocities due to the reference scale being distorted. A solution can be to reposition the reference scale, but this has to be done manually in Tracker, and is time consuming. Another solution can be to use a narrower lens positioned a longer distance away, though this was not feasible.



(a) 30 frames per second.



(b) 1000 frames per second.

Figure 4.3: Still images from videos recorded at different frame rates.

Another important limitation was the frame rate of the video (FPS, frames per second). If the objects in a video recording move too much during the exposure of a single frame, the video becomes blurred. This made it difficult to distinguish the flow front in videos with lower frame rates. Recording video at a higher frame rate was a solution to this issue. Figures 4.3a and 4.3b show the difference of videos recorded at 30 FPS and 1000 FPS. Video resolution is less important, as long as it is high enough to capture the details wanted. The 1000 FPS video is shot at a lower resolution than the 30 FPS video.

4.2.2 Flow Height Data Analysis

The flow height was measured continuously during the test run. In general, it rapidly increased after the flow front, before rapidly decreasing after reaching a peak. For the purpose of calcu-

lating discharge and comparison of flow heights from different tests, the peak value for the flow height was used. Figure 4.4 shows how the peak flow height was selected from test data.

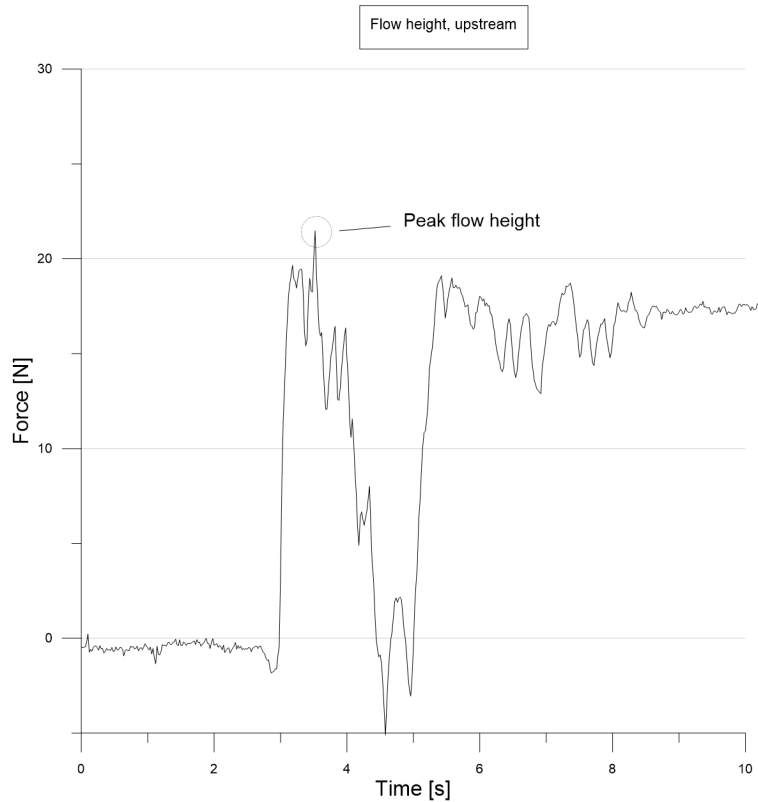


Figure 4.4: Example of flow height sensor data, showing how peak flow height is selected.

The flow height data is also used to calculate the velocity of the flow. The distance between the sensors is known, and by calculating the time it takes for the flow to pass the different sensors, the average velocity between two sensors can be calculated. The flow is considered to have reached a sensor the moment the recorded flow height is equal to or above 1 mm.

From the flow height data and velocity data, it is possible to calculate the flow discharge as

$$\text{"Discharge"} = \text{"Velocity"} \cdot \text{"Max flow height"} \cdot \text{"Channel width"} \quad (4.3)$$

4.2.3 Force Sensor Data Analysis

The force acting on the rectangular pillar was measured continuously during a test run. In general, the peak force during the impact was taken as the maximum impact force. Figure 4.5 illustrates how the maximum impact force was selected.

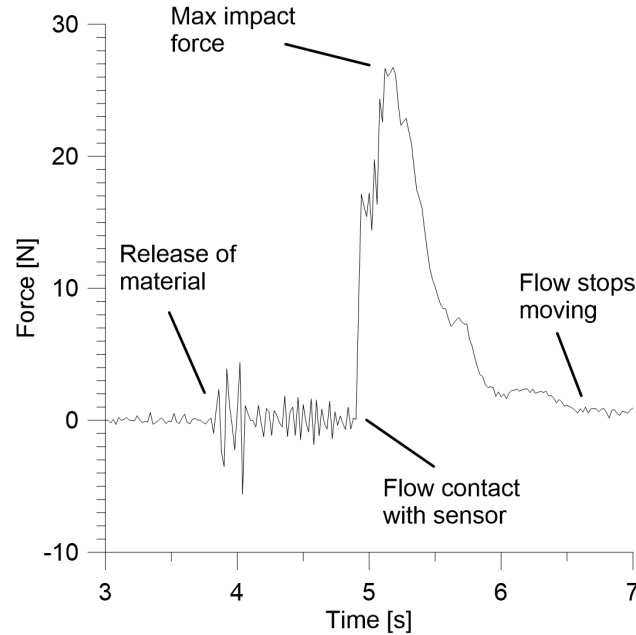


Figure 4.5: A typical force sensor signal. In general, the peak impact is taken as the max impact force. The opening of the mixer and release of the material is visible due to the vibrations it causes in the model.

As the flow will follow the angle of the runout channel (see figure 3.9b), the recorded impact force was corrected as follows:

$$\hat{F} = \frac{F}{\cos \alpha} \quad (4.4)$$

\hat{F} is the corrected force, F is the measured impact force and α is the slope angle.

An estimation of the impact pressure can be calculated by using the flow height. Measurement of the flow height during the impact of the force sensor was not recorded, but for a rough estimation, the maximum flow height recorded by the last flow height sensor 1 m before the force sensor can be used. Then the impact pressure can be calculated as

$$p = \frac{\hat{F}}{h_{max} \cdot w_s} \quad (4.5)$$

with p being the impact pressure, h_{max} being the maximum recorded flow height and w_s the width of the force sensor.

4.3 Coefficients for Debris Flow Impact Formulas

The coefficients k and a in the hydraulic formulas (equations (2.20) and (2.21)) could be calculated from the flume model test results.

Chapter 5

Results

In this chapter, the results from the experiments are presented.

5.1 Flow Behaviour Tests

The testing of the flow properties of the material consists of 6 fall cone-, quickness- and viscometer tests, using two different soils and six different concentrations of solids.

5.1.1 Fall Cone Test Results

The results from the fall cone tests are shown in table 5.1. For tests with indentation in the range of 16–20 mm, the shear strength is 0.10 kPa. For 4 of the 6 tests, the cone sank to the bottom of the bowl, indicating a lower shear strength than 10 kPa.

Table 5.1: Results from the fall cone tests. "-" indicates the material was too liquid for an indentation.

Test number	Test name	Average Indentation	Remoulded shear strength
		[mm]	[kPa]
1	C30S1	-	<0.10
2	C35S1	-	<0.10
3	C40S1	-	<0.10
4	C45S1	19	0.10
5	C20S2	-	<0.10
6	C30S2	19	0.10

5.1.2 Quickness Test Results

The results from the quickness test are shown in table 5.2. The quickness value is calculated using equation (2.1). As seen, the quickness value is decreasing with C_s and the size of the clay fraction of the soil. $C_s = 45\%$ for soil 1 was equivalent to $C_s = 30\%$ for soil 2 in terms of quickness value. $C_s = 20\%$ of soil 2 was equivalent to $C_s = 30\text{--}35\%$ for soil 1.

Table 5.2: Results from the quickness test

Test number	Test name	Deformation height	Lateral spread	Quickness value
		[mm]	[mm]	[%]
1	C30S1	4	840	96
2	C35S1	7	640	93
3	C40S1	15	410	85
4	C45S1	23	280	77
5	C20S2	5	810	95
6	C30S2	23	270	77

5.1.3 Viscometer Test Results

The raw data from the dynamic response test consists of torque measurements at different rotational speeds. Five out of six tests were successful. For test number 5 (C20S2), the torque reading was 0 for all rotation speeds. This test was discarded from further analysis. The test results for the successful tests are shown in figure 5.1.

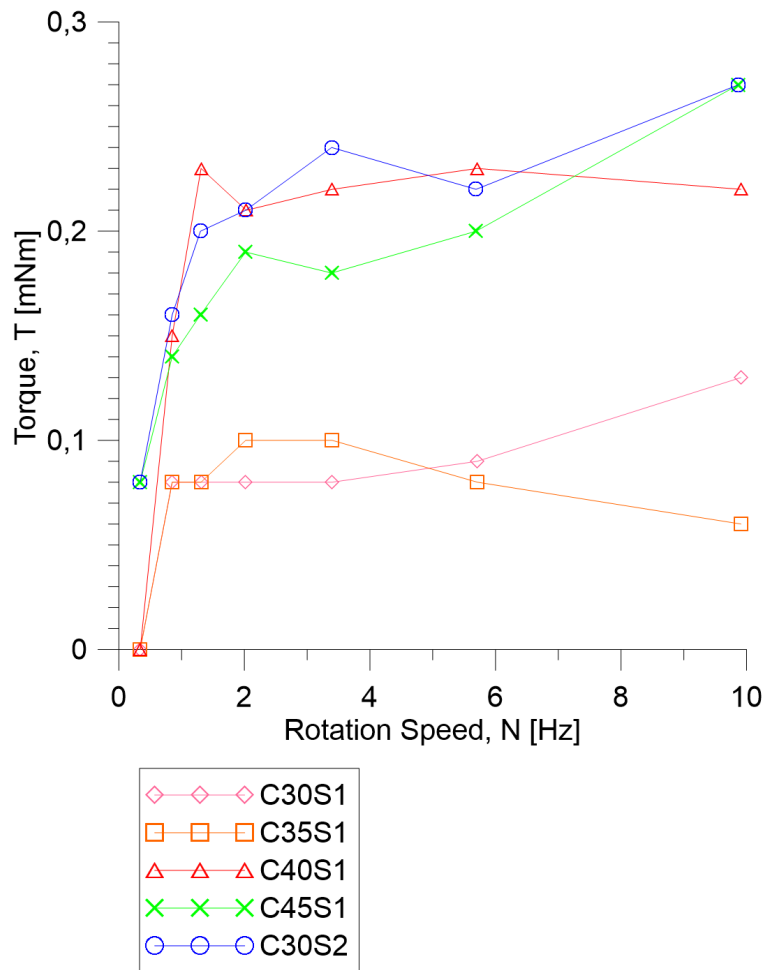


Figure 5.1: Results from the dynamic response test. Torque readings for different rotational speeds.

The results from the dynamic response was then fitted to a curve using MATLAB, as described in section 4.1. For test number 1, 3, 4 and 6, all points were used in the fitting. In the case of test number 1, a constriction of no negative values for the coefficients had to be applied in order to get positive values for G_{HB} . Negative values would lead to negative τ_y . This was undesired, as it would mean the parameters could not have been used for further use in numerical modeling. It also does physical sense for the yield stress to be negative. The best fit parameters are for all tests are shown in table 5.3. The table also includes the calculated Herschel-Bulkley parameters.

Table 5.3: Best-fit curve parameters and the corresponding Herschel-Bulkley parameters.

Test number	Test name	Points used	H_{HB} [Nm s ^{<i>J</i>}]	<i>J</i> [-]	G_{HB} [Nm]	K [Pa s ^{<i>n</i>}]	<i>n</i> [-]	τ_y [Pa]
1	C30S1	All	5.53E-05	0.0335	4.36E-07	2.514	0.335	0.037
2	C35S1	Three middle	3.92E-05	0.375	4.13E-05	1.600	0.375	3.486
3	C40S1	All points	2.68E-05	0.406	1.67E-04	3.194	0.406	4.708
4	C45S1	All points	7.39E-05	0.442	6.18E-05	2.535	0.442	5.216
6	C30S2	All points	5.33E-05	0.5299	1.07E-04	1.469	0.530	9.012

5.2 Flume model test results

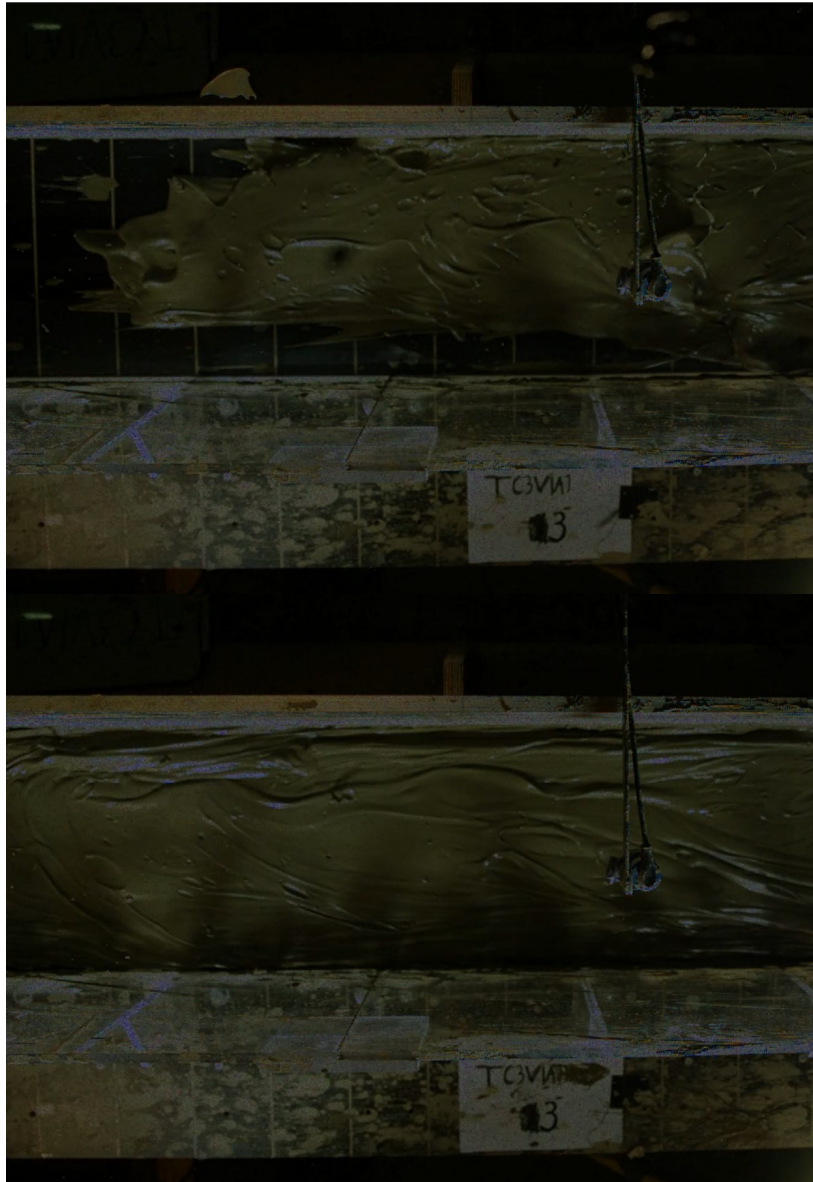


Figure 5.2: Screenshots from high-speed recording of test set 6 (Q77S1V20), illustrating that the composition of the flow remains the same in the front and the middle of the flow, and that no noticeable segregation occurs during the test.

The debris flow tests in the flume model behaved as a viscous, homogeneous flow. Once the mixer was opened, the material flowed rapidly down the slope, without exhibiting observable segregation of the solid material. See figure 5.2 for screenshots of the high-speed recording, illustrating the flow behaviour. The flow appeared to move as a plug-like laminar flow, showing

little turbulence. When it impacted the force sensor, the flow became more turbulent in the impact, and is splashing upwards and to the sides (see figure 5.3). The deposition length exceeded the deposition area in most of the tests. Because of this, a comparison of deposition lengths was not made.

In total, 22 test repetitions were carried out. Two different release volumes and 3 different quickness values was used. One test had to be discarded due to a mistake when mixing the material. Another revealed that the material in the second batch (soil 2) was different. While it showed the effect of an increased clay fraction in the test material, the results could not be compared to the rest. Because of this the test is ignored from all assessments except those regarding the effect of the clay content. The remaining 20 test repetitions makes up the six core test sets (set 1–6) and two single-repetition tests (test set 7 and 8). Test 7 and 8 are only used for assessing the effect of using a different soil with the same quickness value.

Pore pressures were also recorded, but there were some technical issues with the sensors. Due to limited time available, the pore pressure data has not been analyzed properly.

5.2.1 Velocity and Flow Height

When analyzing the results, the focus was put on the processes at the end of the runout channel. This gave the flow time to stabilize after the release and reach more of a steady-state flow.

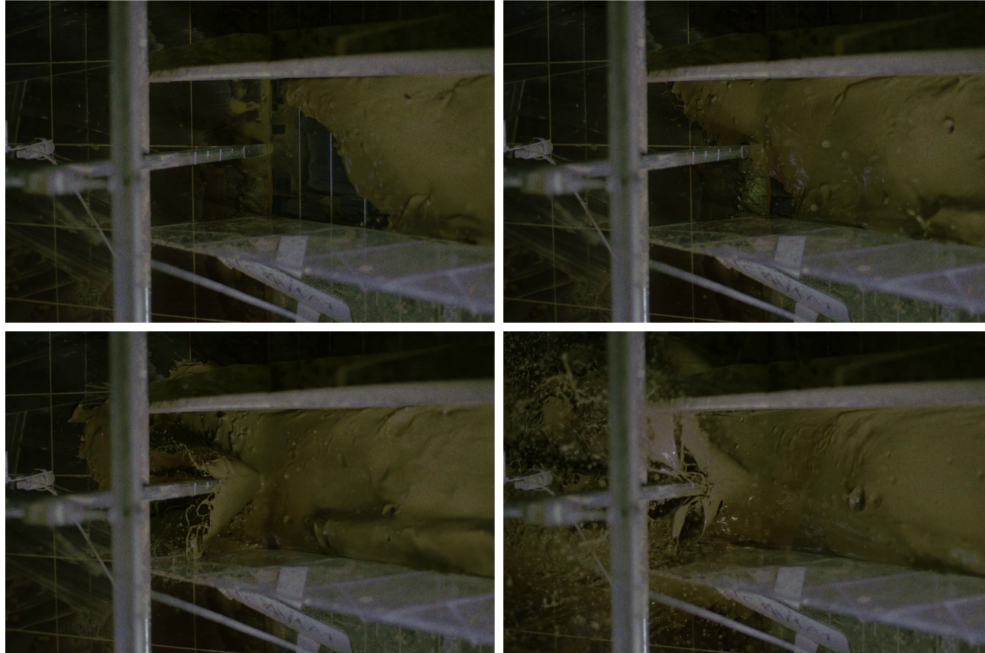


Figure 5.3: Screenshots from high-speed recording of test set 6 (Q77S2V40), showing the interaction with the force sensor. The flow becomes highly turbulent and is spraying upwards as it hits the sensor.

Due to a technical mistake, many of the video recordings were recorded at lower framerates than intended (30–60 FPS instead of 120–240). Due to the rapid velocity of the flow, this made accurately calculating the velocities from these videos difficult. The placement of cameras also varied, making analyses of the flow velocities from these videos challenging. In order to have a more systematic method for calculating the velocities, the flow height data was used instead. The data from the flow height sensors located 2 and 1 m before the end of the channel is used to calculate an average velocity as the flow approaches the end of the runout channel. Unless otherwise specified, this average velocity is used in the assessments. The results from the video analyses can be found in the in table B.1 in the appendix.

Table 5.4: Velocities, flow heights, calculated flow discharges and Froude numbers. Discharge and Froude number is calculated using the maximum flow height recorded 1 m before the end of the runout channel.

Test name	Velocity, average [m/s]	Max flow height, 1 m before end [mm]	Max flow height, 2 m before end [mm]	Flow discharge [m ³ /s]	F_r [-]
Q93S1V40-1	5.00	25	40	0.0375	10.10
Q93S1V40-2	6.25	29	33	0.0544	11.72
Q93S1V40-3	4.17	24	33	0.0300	8.59
Q85S1V40-1	4.55	26	33	0.0355	9.00
Q85S1V40-2	5.00	25	28	0.0375	10.10
Q85S1V40-3	4.55	23	25	0.0314	9.57
Q77S1V40-1	4.55	31	31	0.0423	8.24
Q77S1V40-2	4.17	26	32	0.0325	8.25
Q77S1V40-3	5.00	26	31	0.0390	9.90
Q77S2V40-2	5.00	26	32	0.0392	9.87
Q95S2V20-1	4.55	17	23	0.0237	11.01
Q95S2V20-2	4.55	20	23	0.0278	10.16
Q95S2V20-3	4.17	16	22	0.0196	10.63
Q85S1V20-1	5.00	17	21	0.0255	12.24
Q85S1V20-2	5.00	16	19	0.0240	12.62
Q85S1V20-3	5.00	16	21	0.0240	12.62
Q77S1V20-1	2.50	21	25	0.0157	5.52
Q77S1V20-2	2.78	16	19	0.0129	7.12
Q77S1V20-3	3.33	22	22	0.0225	7.10
Q77S2V20-1	4.17	16	18	0.0198	10.57

In general, velocities are high and flow heights are low. This leads to relatively high Froude numbers, in the range of approximately 7–13. Table 5.4 gives some velocity and flow height data, as well as calculated discharges and Froude numbers for all successful tests. Typical flow height data is shown in a plot in figure 5.4.

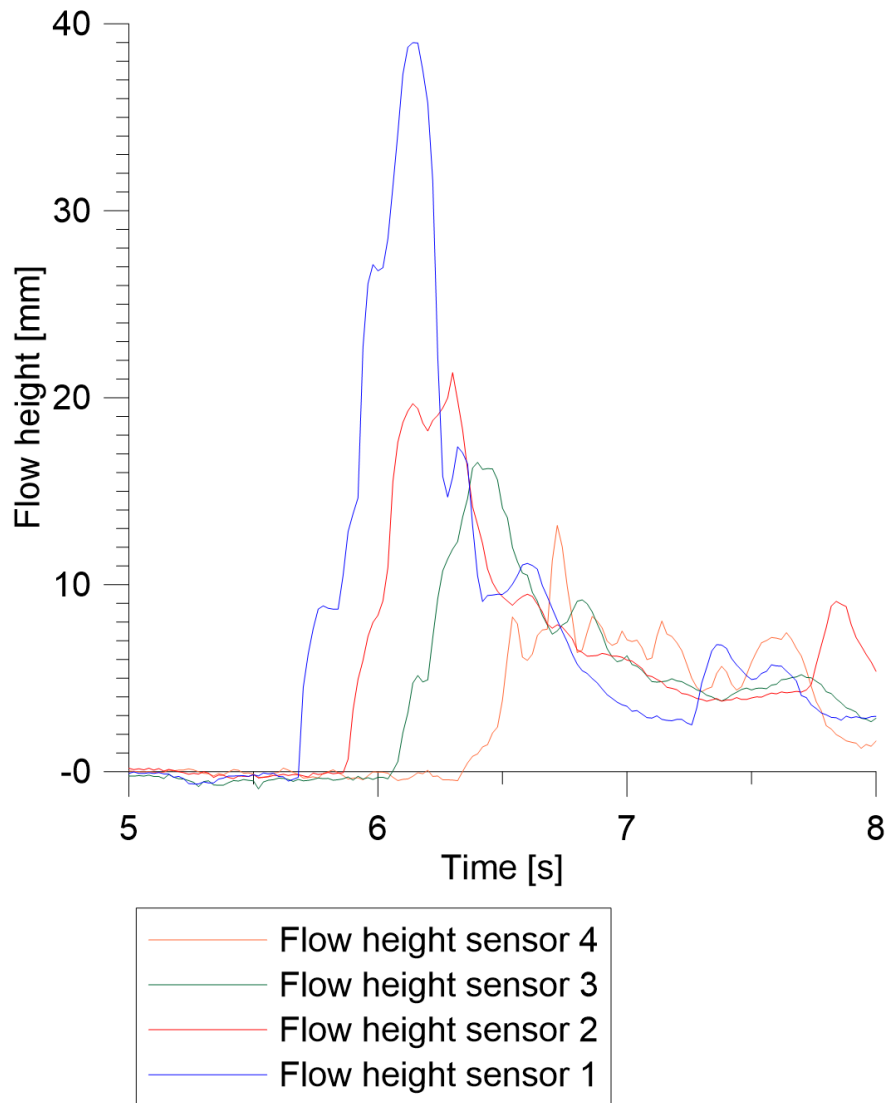


Figure 5.4: Typical flow height results, from test Q85S1V20-1.

5.2.2 Impact Force

The measured impact forces range from approximately 11–45 N, after being corrected for impact angle. Results from each test can be seen in table 5.5. By using the flow heights recorded 1 m before the impact, impact pressures were also calculated, these were found to be in the range of approximately 31–74 kPa.

Table 5.5: Corrected impact force values, as well as calculated impact pressure for all successful tests.

Test name	Max impact force, recorded [N]	Max impact force, corrected [N]	Calculated impact pressure [kPa]
Q93S1V40-1	34.51	38.73	61.97
Q93S1V40-2	39.98	44.87	61.89
Q93S1V40-3	34.49	38.71	64.52
Q85S1V40-1	43.04	48.30	74.32
Q85S1V40-2	37.36	41.93	67.09
Q85S1V40-3	38.79	43.54	75.71
Q77S1V40-1	20.32	22.81	29.43
Q77S1V40-2	26.74	30.01	46.17
Q77S1V40-3	20.3	22.78	35.05
Q77S2V40-2	34.21	38.39	58.71
C95S2V20-1	17.03	19.11	43.97
C95S2V20-2	19.70	22.11	43.36
C95S2V20-3	24.11	27.06	69.13
Q85S1V20-1	20.71	23.24	54.69
Q85S1V20-2	32.30	36.25	90.63
Q85S1V20-3	25.00	28.06	70.15
Q77S1V20-1	9.60	10.77	20.62
Q77S1V20-2	11.68	13.11	33.79
Q77S1V20-3	15.57	17.47	31.11
Q77S2V20-1	13.70	15.38	38.85

5.2.3 Coefficients for use in Analytical Solutions

Equations 2.20 and 2.21 was used to calculate the hydrostatic coefficient, k , and the hydrodynamic coefficient, a , respectively.

Table 5.6: Calculated analytical hydrostatic and hydrodynamic coefficients for all successful test repetitions.

Test name	Max impact force, corrected [N]	Impact pressure [kPa]	Hydrostatic k [-]	Hydrodynamic a [-]
Q93S1V40-1	38.73	61.97	155.35	1.52
Q93S1V40-2	44.87	61.89	133.75	0.97
Q93S1V40-3	38.71	64.52	168.47	2.28
Q85S1V40-1	48.30	74.32	169.79	2.10
Q85S1V40-2	41.93	67.09	159.41	1.56
Q85S1V40-3	43.54	75.71	195.55	2.14
Q77S1V40-1	22.81	29.43	53.59	0.79
Q77S1V40-2	30.01	46.17	100.26	1.47
Q77S1V40-3	22.78	35.05	76.11	0.78
Q77S2V40-2	38.39	58.71	146.83	1.51
C95S2V20-1	19.11	43.97	187.84	1.55
C95S2V20-2	22.11	43.36	157.98	1.53
C95S2V20-3	27.06	69.13	328.00	2.90
Q85S1V20-1	23.24	54.69	191.11	1.27
Q85S1V20-2	36.25	90.63	336.48	2.11
Q85S1V20-3	28.06	70.15	260.43	1.64
Q77S1V20-1	10.77	20.62	55.70	1.83
Q77S1V20-2	13.11	33.79	122.91	2.43
Q77S1V20-3	17.47	31.11	78.16	1.55
Q77S2V20-1	15.38	38.85	160.58	1.21

As seen in table 5.6, values for k are high, ranging from around 55 to about 330 at the most. The hydrodynamic a are ranging from about 1 to about 3.

5.2.4 Impact Force of a Solid Clump of Soil

In one of the test repetitions (Q77S2V40-2), there was a clump of soil (approximately 20-30 mm in diameter) present in the released material. It arrived at the force sensor well after the flow front, so it was not considered to have had an effect on the results. See figure 5.5 for pictures of the clump taken from the high-speed recording.



(a) A soil clump in the flow material.



(b) The soil clump as it approaches the force sensor.



(c) Impact of the soil clump on the force sensor.

Figure 5.5

The impact was visible on the signal from the force sensor (see figure 5.6). The recorded impact force of the clump was 67 N, almost double of the max impact force from the slurry (34 N).

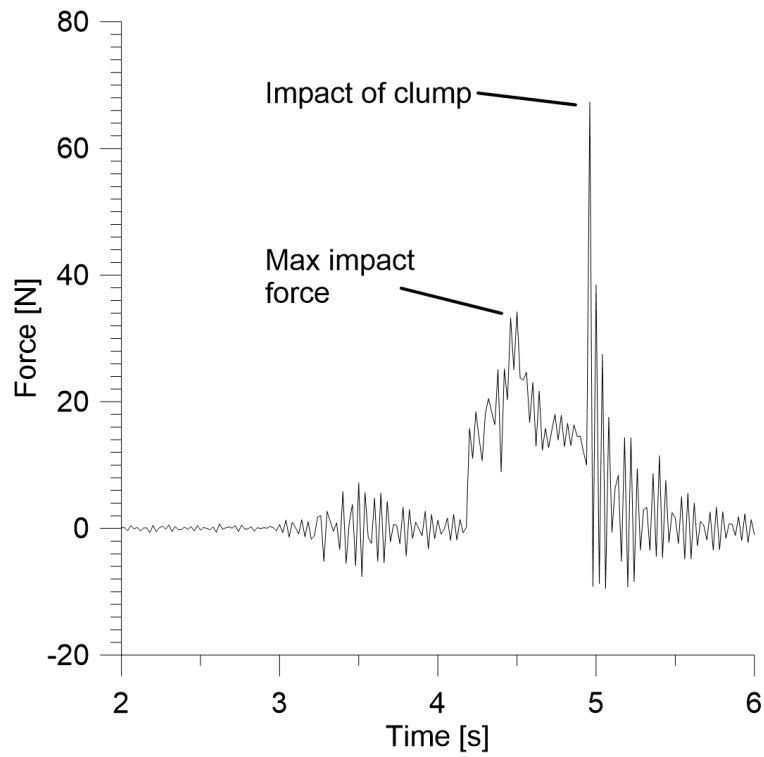


Figure 5.6: The signal from the force sensor for test Q77S2V40-2. Notice the impact force being significantly larger than the max impact force of the fluid

Chapter 6

Discussion

This chapter presents a discussion of the results from the laboratory testing of a fine grain rich debris flow.

6.1 Quickness and Remoulded Shear Strength

Results from the fall cone tests and quickness tests was well within the limits of quick clay landslides proposed by Thakur and Degago (2012), which was $c_{ur} < 1\text{kPa}$ and $Q > 15\%$. The quickness value increased with increasing C_s and with increasing clay fraction.

6.2 Viscometer test

A rotational viscometer was used to find Herschel-Bulkley parameters for for four different values of C_s for soil 1, and one value of C_s for soil 2.

In figure 6.1, flow curves are plotted using the Herschel-Bulkley parameters calculated from the viscometer test results. Selected results from previous viscometer testing of fine grained soil is also plotted. The results from Major and Pierson (1992) were selected based on similarity in C_s . Results from Adamson (2017) were selected based on similarity in material and c_{ur} .

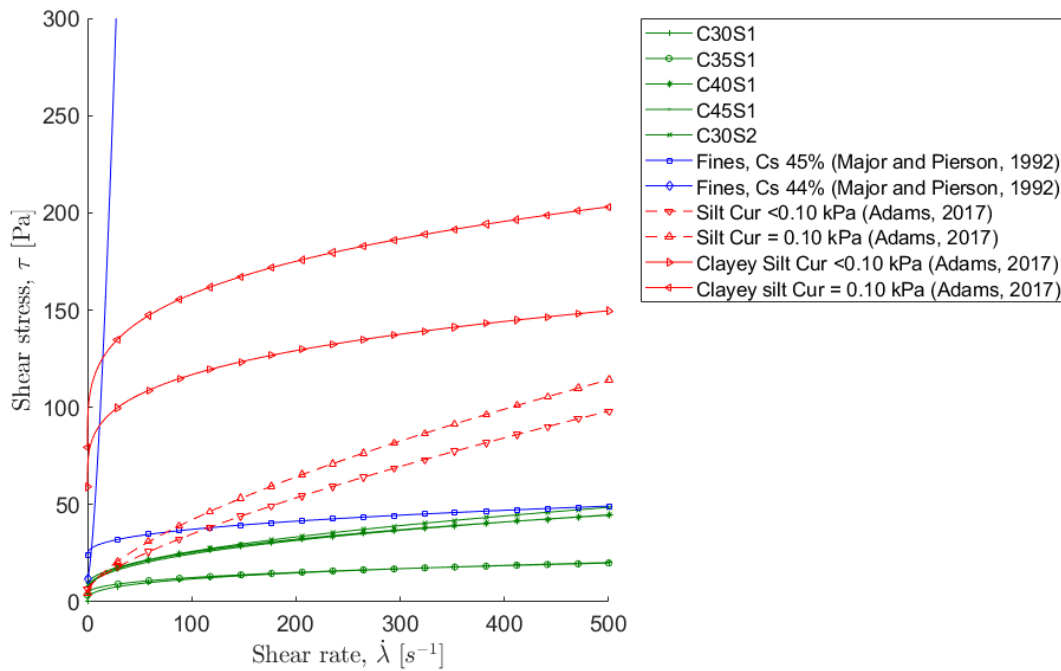


Figure 6.1: Flow curves plot of the results from this thesis with select flow curves from Major and Pierson (1992) and Adamson (2017).

The results further confirms previous findings that mixtures of fine grained soils behaves as a non-Newtonian fluid. The results shows shear thinning behaviour, and appears to have a yield stress. This shows that the Herschel-Bulkley model is an appropriate rheological model for this type of material.

The material in tests C45S1 and C30S2 had the same quickness value ($Q = 77\%$), but the soil used was different. C30S2 and C30S1 had the same C_s , but different quickness values ($Q = 96\%$ for C30S1). When comparing the Herschel-Bulkley flow curves (see figure 6.2), C30S2 is closer to C45S1 than C30S1 in behaviour. This suggests that quickness is an important parameter, and that concentration is less important, at least for this soil.

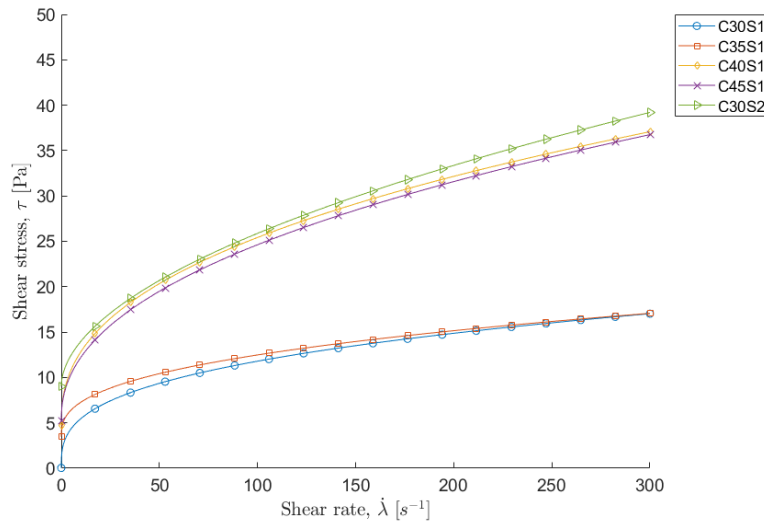


Figure 6.2: Herschel-Bulkley flow curves for all tests. The equation for the Herschel-Bulkley model is $\tau = \tau_y + K\dot{\gamma}^n$.

The shape of the curves coincides well with the results from Major and Pierson (1992) and Adamson (2017). However, there are some differences in the values of τ_y . The Herschel-Bulkley yield stresses found in the experiments were low, with values ranging from 0.037–9.012 Pa. This is a lower than Major and Pierson (1992) who found the yield stress to be 12 Pa for $C_s = 44\%$, increasing rapidly with concentration ($C_s = 52\%$ gave a yield stress of 163, see table 2.1).

Interestingly, the Herschel-Bulkley yield stresses for the silt material in Adamson (2017) are similar to the results found in the experiments conducted in this thesis. This can be seen in figure 6.1. Adamson (2017) excluded these results from further assessment due to observed segregation during the viscometer testing. This was not observed during the tests conducted in this thesis. However, segregation was observed in the bowl containing the leftover material. See figure 6.3 for an example. This behaviour was observed for all values of C_s . It was initially expected that there would be less segregation when using soil 2, as it had a higher clay content, but this was not observed to be the case.

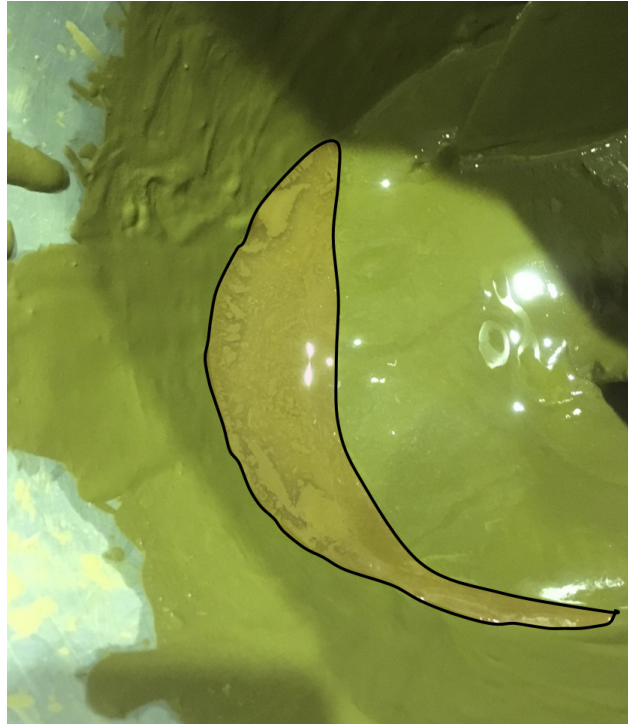


Figure 6.3: Picture of inside the bowl with leftover material from a viscometer test. Notice the water visible in the shaded region.

The low values of the Herschel-Bulkley yield stresses is a consequence of low torque readings during the dynamic response test. For the tests of $C_s = 30\%, 35\%$ and 40% , the torque reading was zero at the lowest rotation speed (see figure 5.1). A possible explanation for low torque readings is slippage between the spindle and the material. This was encountered by Adamson (2017) for materials with higher values of c_{ur} . However, this was encountered for the materials with the lowest C_s and values of C_{ur} in this case. This makes it unlikely that slippage due to high C_{ur} is the reason for zero torque readings at the lowest speed setting.

It is possible that the configuration used for the viscometer was not sensitive enough for the lower concentrations. A bigger geometry of the cylinder and spindle could have increased sensitivity. As the largest outer cylinder was missing for the instrument, this was not tested. A narrow gap configuration with a bigger spindle was tested. However, this configuration had problems reaching a stable torque reading. A possible reason for this is that the gap was too small in relation to the grain size diameter of the material.

The curve fitting of the dynamic response was challenging in some cases. See figure 6.4 for an

example of different curve fits. The test in the figure is one of the tests where the torque reading was zero for the lowest speed. As seen, it is challenging to select the curve with the closest fit to the data.

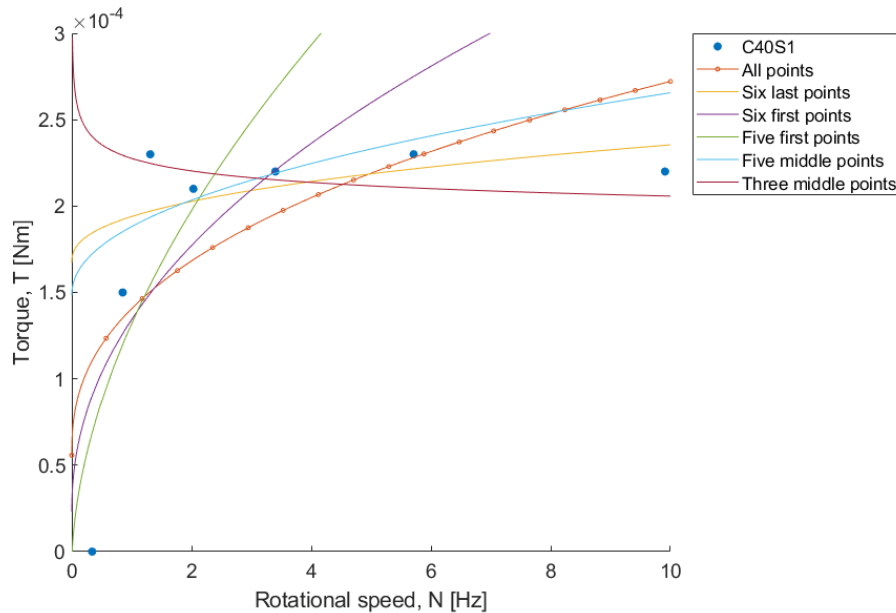


Figure 6.4: Curve fit of test C40S1. The curve fitted to all points was considered the best fit

It was decided to include the first points in the curve fitting if possible, even if the registered torque was unrealistically low. This was done in order to not overestimate the stress in the lower regions of shear rate. In some cases, one or more of the coefficients in the curve fit became negative. This could lead to either non-real parameters or negative yield stress in the Herschel-Bulkley model, which is not realistic. It would also be problematic if the parameters were to be used in numerical modeling.

6.3 Physical Modeling of Debris Flow

To evaluate the physical modeling of a fine rich, viscous debris flow, the observations made in these tests are compared to observations of real debris flow, as well as other small-scale tests.

6.3.1 Velocity

As calculated in section 3.3.3, the velocities in the flume model should be in the range of 2.24–3.35 m/s. As seen in table 5.4, the measured velocities are in the range of 2.50–6.25 m/s, which translates to velocities in the range of 11–28 m/s. An average velocity of 4.48 m/s can be scaled up to 20 m/s. Even though alpine debris flows are characterized by velocities higher than 10 m/s, a velocity of 20 m/s is still quite high.

The slope angle has a big impact on the flow velocity (Huang et al., 2007), and the slope angle used in the experiments was very steep at 27°. The reason this slope angle was chosen was to ensure that the material would flow properly at the lowest quickness values. Small volumes of material was tested on a flat plastic screen at different slope angles before testing, and for most concentrations it was flowing slowly. Still, it is clear when analysing the test results that the slope angle could have been decreased, and this would have decreased the velocities.

No in-depth analysis of how the velocity is varying throughout the flume was conducted. Due to the challenges and poor video data quality, a complete velocity profile for each test could not be developed. Calculation of velocity profiles from videos requires a high frame rate. It was deemed to not be worth the time and effort it would take to analyze the videos in detail, due to the low frame rates on certain videos. The velocity was instead calculated at selected points from different videos (results in table B.1 in the appendix), and the values did not vary greatly from the calculated average from the flow height sensors.

6.3.2 Flow Height

The measured flow heights are in the range of 16–40 mm, which translates to a scaled up range of 0.32–0.8 m. The average recorded value was 24 mm, which scales up to 0.48 m. This is within the range of the Alpine debris flows mentioned previously (0.2–1.5 m), but in the lower end.

6.3.3 Froude Number

The flow height and velocity data was used to calculate the Froude number for each test. As seen in table 5.4, the Froude numbers are quite high (approximately 7–13). This is much higher than the upper limit of 3 suggested by Hübl et al. (2009) for laboratory results. It is also higher than the range of 2.61–7.14 given earlier for alpine debris flows.

6.3.4 Impact Forces

The impact forces measured range from about 11 N to about 45 N. By using the last recorded flow height and the width of the flow height sensor to calculate an impact area, the impact pressure was calculated to be ranging from 20 to 62 kPa. When scaled up, this equals a full-scale impact pressure of 400 kPa to 1240 kPa. This is significantly higher than the 200 kPa mentioned in Bugnion et al. (2012).

The force sensor is built on the assumption that the resultant force is acting on a point at a distance from the rotation point equal to the distance from the rotation point to the force transducer. This point is located 15 mm from the bottom of the channel. If the pressure distribution from the incoming flow is assumed to be constant in the vertical direction, this means the flow height has to be 30 mm for the force measurement to be correct. The recorded flow heights are in the range of 16–40 mm. This leads to a measurement error of up to 2%, which is considered acceptable.

During one of the tests, a 20–30 mm sized clump in the material hit the force sensor directly. The impact force of this clump was measured to be 67 N, which is twice the measured max impact force of the fluid material. 67 N would scale up to 536 kN, which is close to previously measured impact forces from boulders in debris flows. It also suggests that the impact of debris carries more destructive power than the dynamic pressure of the slurry.

6.4 Analytical models for estimating impact forces

The measured impact forces was back calculated using the hydraulic formulas presented in section 2.4.

The hydrostatic formula requires the flow height as input, and since the flow height could not be measured at the exact location of the force sensor, the flow heights from the flow height sensor positioned 1 m before it was used. The maximum flow heights recorded in general barely decreased between the sensors (see table 5.4). Considering this, the values were used to estimate the impact flow height.

The hydrostatic formula introduces a coefficient, k that relates the static pressure of the flow to the impact pressure of a moving flow. The values for k was calculated to be in the range of 54–336. This is significantly higher than the range of 2.5 to 11, as suggested in the literature. The only debris flow parameters that are used for input in the hydrostatic formula is the density of the flow and the flow height. Velocity and all other parameters are included in the coefficient k . In the experiments covered in this thesis, the observed velocities were quite high, and the observed flow heights quite low. This will result in high values for the coefficient k , which also suggests that the dynamic pressure is dominating the static pressure. This confirms that the hydrostatic formula is less useful when used for high-velocity flows (Proske et al., 2011).

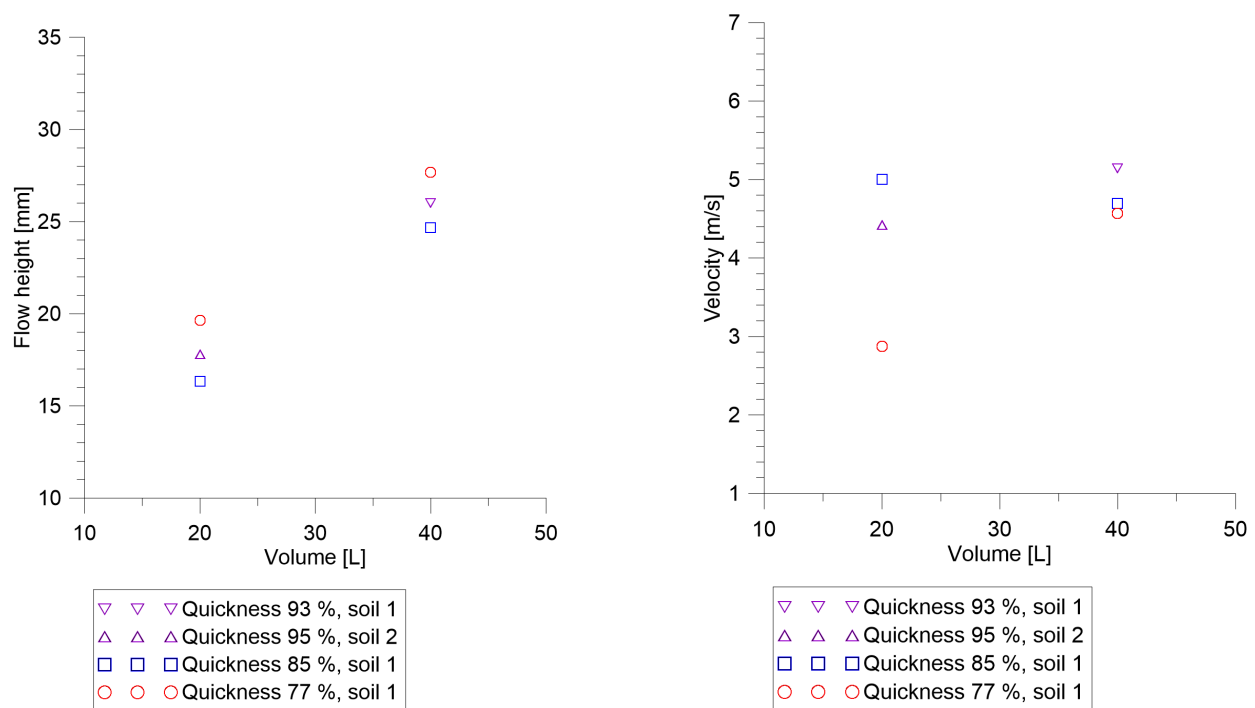
For the hydrodynamic formula, impact velocity and flow height was needed. For velocity, the average velocity calculated from the flow height data was used. As mentioned earlier, the velocity did not appear to vary much throughout a single test, and it was assumed this was a good estimate for the impact velocity of the flow.

In the hydrodynamic formula, the coefficient a is used to take into account obstacle and debris flow characteristics. The values of a found to range from 0.79 to 2.90 (see table 5.6), with an average of 1.66. This is well within the lower range of 0.4 to 12 reported in the literature, and further confirms previous findings that the hydrodynamic model works best for high velocities and Froude numbers (Proske et al. (2011); Scheidl et al. (2013)).

6.5 Effect of Flow Volume in the Flume Model

Results from test set 1–6 also shows the effect of changing the released flow volume. For each quickness value of the flow material, two different volumes were tested, 40 L and 20 L.

Figure 6.5a shows the effect of increasing the release volume has on the flow height. The flow heights are higher for the higher volume, but the results do not show a significant change in the variations within different quickness values (the "grouping" of the data points does not vary with volume). The average increase in flow height across all quickness values is around 50%.



(a) Release volume plotted against max flow height. Average for test set 1–6.

(b) Release volume plotted against velocity. Average for test set 1–6.

Figure 6.5

The velocity results show a different tendency. As seen in figure 6.5b, the maximum velocity did not change significantly. But the velocities are closer together in value for the 40 L test. The differences appear to diminish when the volume is increased. The order of results also changed: for the 20 L test, a quickness value of 85% gave the highest velocity, but for the 40 L test, a quickness value of 93% gave the highest velocity. This can imply that the results should

be very close together for the 40 L test, and that some small variations in how the tests were conducted affected the order.

The tendency of lesser differences with increasing volume continues for the impact force results (see figure 6.6). The exception is the test with quickness 77%. For this test set, the difference compared to the quickness 85% result appear to be the same for both 20 L and 40 L, percentage-wise.

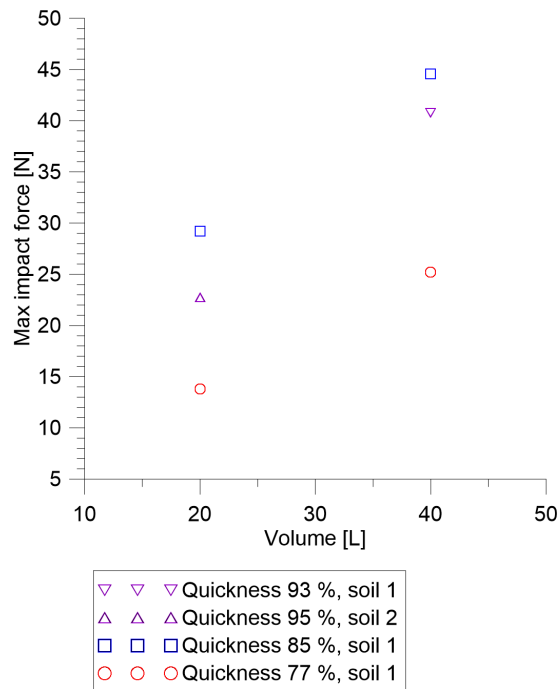


Figure 6.6: Release volume plotted against max impact force. Average for test set 1–6.

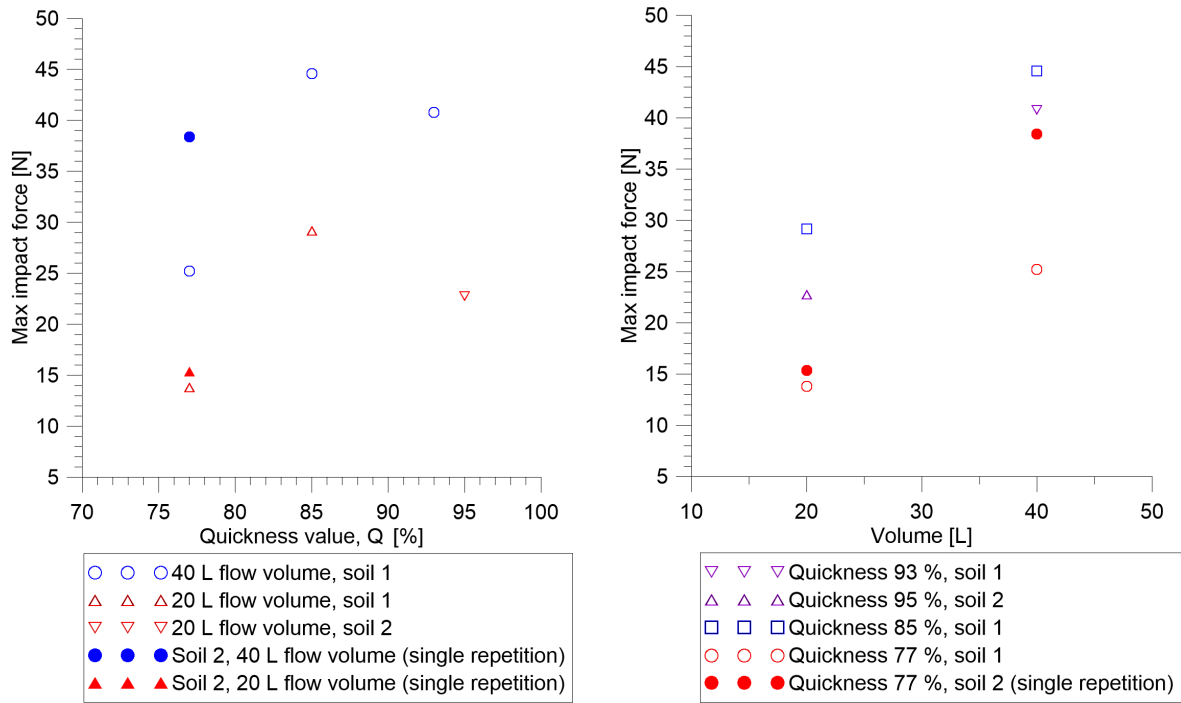
The fact that the test set for quickness 77% has a much lower impact force is contradicting the flow height and velocity results. Q77S1V40, Q93S1V40 and Q77S1V40 all have similar discharges, but the impact force of Q77S1V40 is much lower than the rest (see table 6.1). Similar velocity and flow height should result in a similar impact force. No explanation for this could be found in the test data.

Table 6.1: Results for the 40 L tests, average of test repetitions.

Test name	Flow height [mm]	Velocity [m/s]	Discharge [m ³ /s]	Impact force, corrected [N]
Q93S1V40	26.00	5.14	0.0406	40.77
Q85S1V40	24.67	4.70	0.0348	44.59
Q77S1V40	27.67	4.57	0.0379	25.20

It is assumed that the shape and impact direction for the flow is the same for all tests. If the main part of the flow misses the pillar, the results becomes skewed. However, few observation of the flow impact with the force pillar exist in the test data. The test were also repeated three times. If an imperfect impact is the reason for the lower impact force result, it is unlikely it would happen three times.

In figures 6.7a and 6.7b, quickness and volume is plotted against force for all test sets, including the additional tests conducted for the purpose of evaluating the effect using a different soil for similar quickness values. As seen from these results, the impact force for quickness 77% is significantly higher for the additional test using soil 2.



(a) Quickness plotted against force for all tests, including the additional tests conducted for evaluating the effect of changing the soil.

(b) Volume plotted against force for all tests, including the additional tests conducted for evaluating the effect of changing the soil.

Figure 6.7

One assumption is that the measured impact force results from Q77S1V40 are too low. It is possible that the results from the additional test Q77S2V40 are a better representation for a debris flow with a quickness of 77%. If this assumption is accepted, it would suggest that the effects of variations in quickness value will diminish if the flow volume is increased. However, this is merely a hypothesis based on several assumptions, there is not enough data to make any definite conclusions.

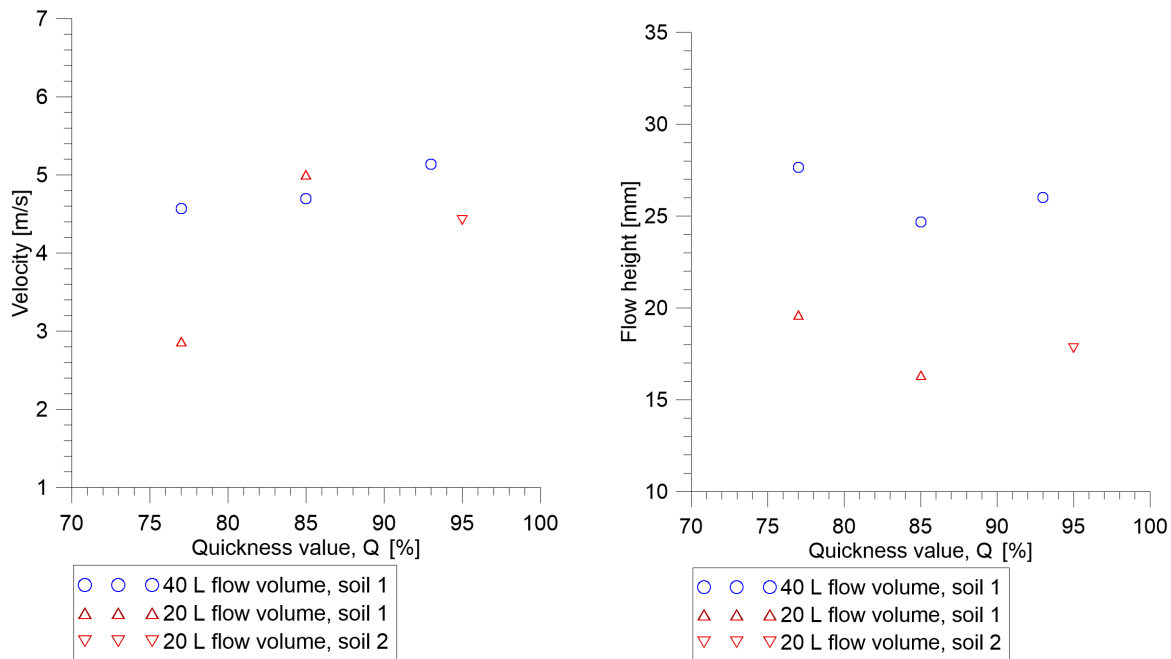
6.6 Effect of Quickness

Results from test set 1–6 shows the effect of variations in quickness value for two different flow volumes (40 L and 20 L).

Figure 6.8b shows the effect the quickness value has on the flow height. For both flow volumes,

40 L and 20 L, the flow height appears to decrease with increasing quickness (decreasing C_s) to a certain point, before increasing again.

For the 20 L test, the effect on the velocity is similar but opposite. As can be seen in figure 6.8a, the velocity increases first with increasing quickness, before decreasing again. The effect is not the same for the 40 L tests. Here, the velocity is slightly increasing when the quickness value is increased.



(a) Quickness plotted against velocity. Average for test set 1–6.

(b) Quickness plotted against max flow height. Average for test set 1–6.

Figure 6.8

The trend of an increase and then decrease with quickness value is also visible in the impact force results. For the 20 L test, the impact force almost doubles when going from a quickness value of 77% to 85%, before decreasing by a lesser amount for the tests of quickness value 93–95%. See figure 6.7a for a plot of the impact force results.

The same trend is also seen for the original 40 L tests. However, if the assumption that the measured impact force is too low is accepted, the increase from quickness value 77% to 85% is less than for the 20 L test. This can be seen from the plot of the results in figure 6.7a.

A high quickness value is indicative of more internal friction and stronger bonds between particles. When the quickness is decreased, grain to grain contact is increased, leading to more internal friction and a more viscous material. This leads to a decrease in velocity, which again leads to a decrease in impact force.

However, the presence of an extremum for the middle quickness value indicates that some effect is counteracting the effect of lowering the quickness value. This effect instead increases the impact forces. This effect could be due to density. A decrease in quickness value is associated with an increase in concentration, which leads to an increase in the density of the flow. However, this hypothesis is somewhat refuted when the additional tests are taken into consideration (see figure 6.9). Test set 7 and 8 (Q77S2V40 and Q77S2V20) have the same quickness value as test set 5 and 6 (Q77S1V40 and Q77S1V20), but very different concentrations ($C_s = 30\%$ and $C_s = 45\%$, respectively) and thus densities.

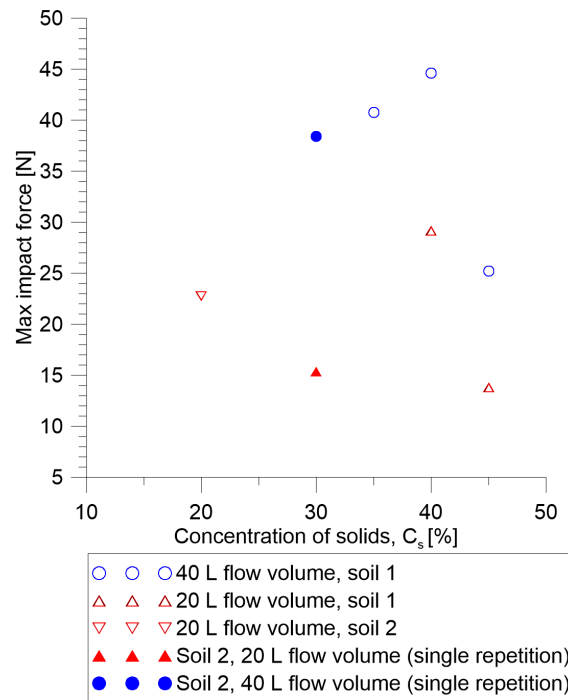


Figure 6.9: C_s vs impact force for all test sets, including the additional test sets. Average values.

More tests should be conducted using different soils and quickness value in order to properly establish the correlations between concentration, density and quickness value.

6.7 Effect of an increased Clay Fraction

The effect of the higher clay fraction in soil 2 compared to soil 1 is significant. This is visible when looking at the quickness values and the associated concentration of solids. To achieve the same quickness value when using soil 2, more water had to be added, decreasing the solid concentration (C_s).

Table 6.2: Quickness values and their associated solid concentrations for soil 1 and soil 2. Quickness values of 93% and 95% were practically the same.

Quickness [%]	C_s , soil 1 [%]	C_s , soil 2 [%]
77	45	30
93	35	
95		20

The fact that soil 2 was different from soil 1 was discovered when a test repetition for test set 1 was carried out. The material in the test had a C_s of 35% and was expected to have a quickness of 93%, which is very fluid. As seen in figure 6.10, the material did not flow at all, and was instead sliding down the slope in big clumps.

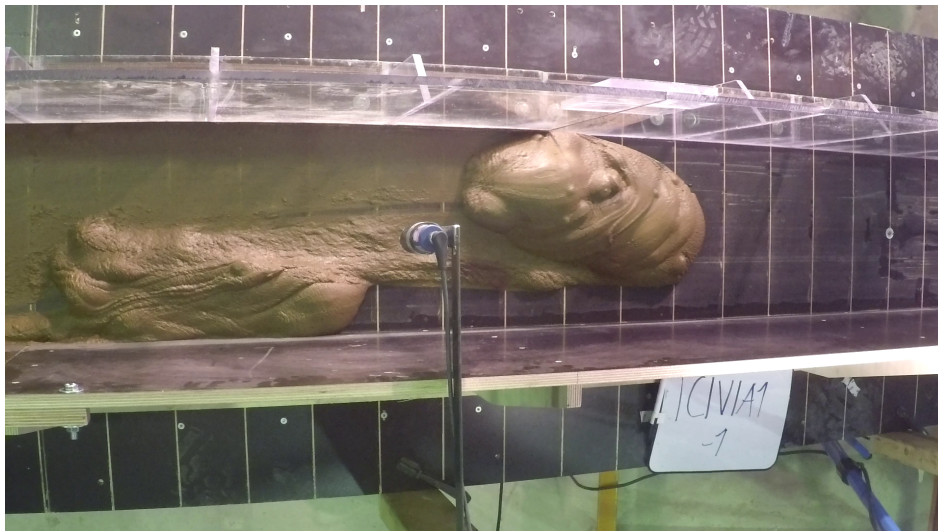


Figure 6.10: Test using soil 2 with a C_s of 35%.

Based on these findings, it is apparent that the clay content has a significant effect on the flow

properties for a given concentration of this material. This is important when discussing solid concentration limits for different flow types. More testing should be done of different soils with different clay contents better define the effect.

Chapter 7

Conclusion and Further Work

7.1 Conclusions

Fine grain rich debris flow have been studied through rheological experiments and physical modeling in a miniaturised flume model.

The rheology has primarily been investigated using viscometer testing. Six viscometer tests were conducted, out of which five was successful. It was shown that fine grain rich soil material behaved as a shear thinning material exhibiting a yield strength, and could be modeled using Herschel-Bulkley rheology.

The shape of modeled Herschel-Bulkley flow curves are similar in shape (similar values for the parameters K and n) to what has previously been reported for fine grain rich soils. The yield stresses found are low compared to what has previously been reported in literature.

22 flume model tests was conducted using the same, fine grain rich material as for the viscometer tests. Velocities, flow heights and impact forces was measured and analysed. Two different soils were used, where the primary difference was the size of the clay fraction. Tests were conducted using different solid concentrations and quickness values.

The flume model is designed as a 1:20 scale model. To ensure correct scaling of the gravitational forces, scaling by Froude number was applied. The scaled up velocities are in the range of 11–28

m/s, which is the upper range of debris flow velocities. The flow heights are in the lower range of expected values, with scaled up values of 0.32–0.80 m. These velocity and flow height values are associated with debris flows in steep alpine terrain.

Coefficients for two simple hydraulic models (static and dynamic) were calculated from the results. The results further confirms that the hydrodynamic model is a better fit when the results are compared to results from the literature.

The results indicate that the effect of variations in quickness value or solid concentration decreases as the flow volume is increased. This trend was observed for the flow velocities and impact forces. But in order to make any definite conclusions about the effect of flow volume, more testing should be conducted.

The effect variations in quickness value appears to be complex. An extremum for the middle quickness value ($Q = 85\%$) was observed in the velocity, flow height and impact force results. For the impact force and velocity, the highest values were measured for the middle quickness value. For the flow height, the lowest value was measured for the middle quickness value. This implies that at least two effects are acting against each other when the quickness value is increased. It is challenging to conclude anything based on the results, more research should be conducted using different soils, quickness values and concentrations.

7.2 Recommendations for Further Work

More viscometric testing should be conducted on debris flow material. Different cylinder and spindle sizes should be trialed in order to find the most effective and accurate way of measuring the viscosity of soil-water mixes. Different types of viscometers should also be looked into, both different rotational ones, or entirely different principles.

The effect of segregation of the tested material in viscometry should be investigated. Especially for courses materials, segregation will be prevalent and more rapid.

The effect of variations in quickness value and concentration should be investigated further. Different soil types with different grain size distributions and origins should be tested. The re-

relationship between quickness, concentrations of solids and also the bulk density of the flow should be tested more.

Lastly, numerical modeling of the flume model results should be conducted, using all available material parameters, including viscosity.

Bibliography

- Adamson, M. (2017). Flow behaviour of fine-grained soils. Master's thesis, Norwegian University of Science and Technology (NTNU).
- Armanini, A. and Michiue, M. (1997). *On the dynamic impact of debris flows*, pages 208–226". Springer Berlin Heidelberg, Berlin, Heidelberg.
- Barnes, H. A. (2000). Measuring the viscosity of large-particle (and flocculated) suspensions — a note on the necessary gap size of rotational viscometers. *Journal of Non-Newtonian Fluid Mechanics*, 94(2):213 – 217.
- Bugnion, L., McArdeell, B. W., Bartelt, P., and Wendeler, C. (2012). Measurements of hillslope debris flow impact pressure on obstacles. *Landslides*, 9(2):179–187.
- Calligaris, C. and Zini, L. (2012). *Debris Flow Phenomena: A short Overview?*, chapter 4. InTech.
- Canelli, L., Ferrero, A. M., Migliazza, M., and Segalini, A. (2012). Debris flow risk mitigation by the means of rigid and flexible barriers — experimental tests and impact analysis. *Natural Hazards and Earth System Sciences*, 12(5):1693–1699.
- Christiansen, L. E. (2013). Flomskred: Litteraturstudie og modellforsøk med voller som sikringstiltak. Master's thesis, Norwegian University of Science and Technology (NTNU).
- Coussot, P., Laigle, D., Arattano, M., Deganutti, A., and Marchi, L. (1998). Direct determination of rheological characteristics of debris flow. *Journal of hydraulic engineering*, 124(8):865–868.
- Coussot, P. and Piau, J. M. (1994). On the behavior of fine mud suspensions. *Rheologica acta*, 33(3):175–184.

- Daido, A. (1993). Impact force of mud debris flows on structures. In *Technical Session B, Proceedings of the XXV IAHR Congress*.
- Dolan, J. (2018). Search teams find 21st victim of montecito mudslide.
- Fiskum, E. (2012). Flomskred – testing av ulike sikringstiltak i modellforsøk. Master's thesis, Norwegian University of Science and Technology (NTNU).
- Grue, R. H. (2015). Rheological parameters of norwegian sensitive clays, focusing on the herschel-bulkley model. Master's thesis, Norwegian University of Science and Technology (NTNU).
- Heirman, G., Vandewalle, L., Van Gemert, D., and Wallevik, O. (2008). Integration approach of the couette inverse problem of powder type self-compacting concrete in a wide-gap concentric cylinder rheometer. *Journal of non-Newtonian fluid mechanics*, 150(2-3):93–103.
- Highland, L. M. and Bobrowsky, P. (2008). *The Landslide Handbook - A guide to Understanding Landslides*. United States Geological Survey.
- Hiller, P. and Jenssen, L. (2009). Modellforsøk med flomskred mot bruer - virkning av bruåpning og ledevoller.
- Hognestad, Å. S. (2017). Effectiveness of a screen type countermeasure against debris flow. Semester project, Norwegian University of Science and Technology (NTNU).
- Huang, H.-P., Yang, K.-C., and Lai, S.-W. (2007). Impact force of debris flow on filter dam. *momentum*, 9(2).
- Huebl, J. and Jaeger, G. (2004). Real scale debris flow experiments at gaschiera/a. *Nice France: European Geosciences Union Google Scholar*.
- Hungr, O., Evans, S., Bovis, M., and Hutchinson, J. (2001). Review of the classification of landslides of the flow type. 7:221–238.
- Hungr, O., Morgan, G. C., and Kellerhals, R. (1984). Quantitative analysis of debris torrent hazards for design of remedial measures. *Canadian Geotechnical Journal*, 21(4):663–677.

- Hübl, J., Suda, J., Proske, D., Kaitna, R., and Scheidl, C. (2009). Debris flow impact estimation. In *International Symposium on Water Management and Hydraulic Engineering*.
- Irgens, F. (2014). *Classification of Fluids*. Springer International Publishing, Cham.
- Iverson, R. M., Logan, M., LaHusen, R. G., and Berti, M. (2010). The perfect debris flow? aggregated results from 28 large-scale experiments. *Journal of Geophysical Research: Earth Surface*, 115(F3).
- Jeong, S. W., Locat, J., and Leroueil, S. (2012). The effects of salinity and shear history on the rheological characteristics of illite-rich and na-montmorillonite-rich clays. *Clays and Clay Minerals*, 60(2):108–120.
- Johnson, A. M. (1970). *Physical processes in geology: A method for interpretation of natural phenomena; intrusions in igneous rocks, fractures, and folds, flow of debris and ice*. Freeman, Cooper.
- Kaitna, R., Rickenmann, D., and Schatzmann, M. (2007). Experimental study on rheologic behaviour of debris flow material. *Acta Geotechnica*, 2(2):71–85.
- Kasim, N., Taib, K. A., Mukhlisin, M., and Kasa, A. (2016). Triggering mechanism and characteristic of debris flow in peninsular malaysia. *American Journal of Engineering Research (AJER)*, 5(4):112–119.
- Kim, Y. (2013). *Study on Hydraulic Characteristics of Debris Flow Breakers and Sabo Dams with a Flap*. PhD thesis, Kyoto University.
- Laache, E. (2016). Model testing of the drainage screen type debris flow breaker. Master's thesis, Norwegian University of Science and Technology (NTNU).
- Liechtenhahn, C. (1977). Die berechnung von sperren in beton und eisenbeton.kolloquium u"ber wildbachsperren. mitteilungen der forstlichen bundesanstalt wien.
- Major, J. J. and Iverson, R. M. (1999). Debris-flow deposition: Effects of pore-fluid pressure and friction concentrated at flow margins. *GSA Bulletin*, 111(10):1424.

- Major, J. J. and Pierson, T. C. (1992). Debris flow rheology: Experimental analysis of fine-grained slurries. *Water Resources Research*, 28(3):841–857.
- Mansurov, N. (2018). What is distortion?
- Pellegrino, A., di Santolo AM, S., and Evangelista, A. Experimental study on the rheological behaviour of debris flow material in the campania region.
- Phillips, C. J. and Davies, T. R. (1991). Determining rheological parameters of debris flow material. *Geomorphology*, 4(2):101–110.
- Proske, D., Suda, J., and Hübl, J. Estimation of design impact forces of debris flows.
- Proske, D., Suda, J., and Hübl, J. (2011). Debris flow impact estimation for breakers. *Georisk: Assessment and Management of Risk for Engineered Systems and Geohazards*, 5(2):143–155.
- Scheidl, C., Chiari, M., Kaitna, R., Müllegger, M., Krawtschuk, A., Zimmermann, T., and Proske, D. (2013). Analysing debris-flow impact models, based on a small scale modelling approach. *Surveys in Geophysics*, 34(1):121–140.
- Schramm, G. (1994). *A practical approach to rheology and rheometry*. Haake Karlsruhe.
- Scotton, P. and Deganutti, A. (1997). Phreatic line and dynamic impact in laboratory debris-flow experiments. In *Proceeding of Debris-flow Hazards Mitigation: Mechanics, Prediction, and Assessment*.
- Takahashi, T. (2014). *Debris Flow: Mechanics, Prediction and Countermeasures*. Taylor & Francis Group, second edition.
- Thakur, V. and Degago, S. (2012). Quickness of sensitive clays. *Géotechnique Letters*, 2(3):87–95.
- Vagnon, F. and Segalini, A. (2016). Debris flow impact estimation on a rigid barrier. *Natural Hazards and Earth System Sciences*, 16(7):1691–1697.
- Vegdirektoratet (2014). Flom- og sørpeskred. Handbook V139, Statens Vegvesen.
- Vegdirektoratet (2016). Laboratorieundersøkelser. Handbook R210, Statens Vegvesen.

Yifru, A., Pradhan, R., Thakur, V., and Nordal, S. (2017). Preliminary study of debris flow impact force on a circular pillar.

Zhang, S. (1993). A comprehensive approach to the observation and prevention of debris flows in china. *Natural Hazards*, 7(1):1-23.

Appendix A

Additional Results from Viscometer Testing

Curve fit parameters for all viscometer tests can be found in table A.1.

Table A.1: Curve fit parameters for all tests. Curves are fitted to the equation $T = H_{HB}N^J + G_{HB}$

Points used	Parameter	C30S1	C35S1	C40S1	C45S1	C30S2
All	H_{HB}	5.39E-04	2.30E-04	8.49E-05	7.39E-05	5.33E-05
	J	0.0519	0.06032	0.4063	0.442	0.5299
	G_{HB}	-4.83E-04	-1.69E-04	5.57E-05	6.18E-05	1.07E-04
Last six (Lowest excluded)	H_{HB}	3.11E-04	-1.05E-04	2.68E-05	1.29E-04	8.49E-05
	J	0.0519	0.06032	0.4063	0.2608	0.3027
	G_{HB}	-2.38E-04	1.96E-04	1.67E-04	1.76E-05	9.77E-05
Six first	H_{HB}	1.71E-03	2.48E-04	1.11E-04	6.58E-05	5.99E-05
	J	0.01546	0.1047	0.4688	0.4582	0.5636
	G_{HB}	-1.65E-03	-1.88E-04	2.31E-05	7.04E-05	9.76E-05
Five first	H_{HB}	2.22E+03	2.98E-04	1.41E-04	8.16E-05	9.30E-05
	J	1.49E-08	0.1396	0.5503	0.4914	0.6148
	G_{HB}	-2.22E+03	-2.36E-04	-8.87E-06	5.40E-05	6.17E-05
Five middle	H_{HB}	2.78E-04	2.92E-05	3.99E-05	8.78E-05	7.23E-05
	J	0.01546	0.1047	0.4688	0.2591	0.325
	G_{HB}	-2.00E-04	5.64E-05	1.48E-04	6.56E-05	1.11E-04
Three middle	H_{HB}	8.00E-05	3.92E-05	8.59E-05	6.04E-05	2.52E-04
	J	0	0.3746	-0.1272	0.2564	0.1505
	G_{HB}	0.00E+00	4.13E-05	1.42E-04	1.04E-04	-6.45E-05

Appendix B

Additional Results from Flume Modeling

Table B.1 contains the velocities as calculated from analysis of the video recordings.

Table B.1: Velocities as calculated from videos. Position is given relative to the force sensor at 0 m.

Test name	Velocity, -2 m	Velocity, at -1 m	Velocity, at 0 m	Framerate
	[m/s]	[m/s]	[m/s]	[FPS]
Q93S1V40-1				
Q93S1V40-2	6.35	5.91		30
Q93S1V40-3	5.76	4.91	3.34	30
Q85S1V40-1	6.29			60
Q85S1V40-2	5.77			60
Q85S1V40-3	5.68			60
Q77S1V40-1	5.28			1000
Q77S1V40-2	4.19			1000
Q77S1V40-3	5.47			1000
Q77S2V40-2			6.25	1000
C95S2V20-1	5.57	4.91		125
C95S2V20-2	4.81	4.8		125
C95S2V20-3		4.26		125
Q85S1V20-1	5.73			60
Q85S1V20-2	5.1			240
Q85S1V20-3	6.38			240
Q77S1V20-1	2.91			1000
Q77S1V20-2	2.16			1000
Q77S1V20-3		2.17		120
Q77S2V20-1			4.8	1000